Co-Pyrolysis of Corn Cob-Husk Blends: Kinetics, Reaction Mechanism, and Products Using TG and Py-GC/MS Analysis

Shaopeng Wang,[a] Yufei Wang,[b] Yadi Hu,[a,*] Zihan Li,[a] Qingyao Zhang,[a] and Shuyan Shan [a]

A comparative study on the pyrolysis of untreated (SA) and NaOH-treated (SB) corn cob-husk blends (1:1, wt%) was conducted to elucidate their kinetic, thermodynamic, and mechanistic characteristics. The NaOH treatment was performed using 10 wt% NaOH solution for 2 h. Thermogravimetric analysis (TGA) was carried out over a temperature range of 50 to 600 °C, and pyrolysis-gas chromatography/mass spectrometry (Py-GC/MS) was performed at 550 °C. The Kissinger-Akahira-Sunose (KAS) and Friedman (FR) isoconversional methods were used to evaluate the activation energies and thermodynamic parameters (pre-exponential factor, Gibbs free energy, enthalpy, and entropy). The minor discrepancies between activation energy (E_α) and enthalpy change (ΔH) (< 6 kJ/mol) for both SA and SB suggest a high potential for biomass energy utilization. Notably, the NaOH treatment resulted in a downward shift in pyrolysis temperature and a lower average activation energy for SB, indicating a thermodynamically more favorable pathway. Mechanistically, the Criado method confirmed that SA follows a three-dimensional diffusion model (D3) initially (Zone I), transitioning to a random nucleation model (F1) beyond approximately 325 °C (Zone II), while SB consistently adheres to the D3 model. Additionally, Py-GC/MS analysis revealed that NaOH treatment, despite reducing bio-oil yield, noticeably enhanced biochar formation.

DOI: 10.15376/biores.21.3.6975-7005

Keywords: Corn cob-husk blends; Co-pyrolysis; Kinetics; Reaction mechanism; Products distribution

*Contact information: a: School of Material and Chemical Engineering, Zhengzhou University of Technology, Zhengzhou 450044, P. R. China; b: School of Materials Science and Engineering, Zhengzhou University, Zhengzhou 450001, P. R. China; *Corresponding author: huyadi1990@163.com*

INTRODUCTION

Fossil fuel consumption is now widely recognized as unsustainable due to its finite reserves and its contribution to over 75% of anthropogenic CO_2 emissions annually, driving unprecedented environmental and climate degradation (Yılbaşı 2025). Given the dual challenges of depleting fossil fuel reserves and deteriorating environmental health, the development of sustainable and environmentally benign energy alternatives has become imperative. Consequently, research into renewable energy sources and fuels has attracted increasing attention. Biomass, as a carbon-neutral and cost-effective renewable hydrocarbon source, presents a viable pathway for producing a diverse range of fuels and chemical feedstocks (Hussain *et al*. 2025).

Corn, a prominent crop globally, primarily yields approximately 5 wt% edible kernels based on total corn plant dry matter, with the remaining 95 wt% constituting non-

edible by-products (Enawgaw *et al.* 2023). These by-products, often viewed as low-value agricultural waste, are significantly underutilized (Silos-Llamas *et al*. 2023). If left unused, burning these residues emits substantial air pollutants, including carbon dioxide (CO_2), carbon monoxide (CO), sulfur dioxide (SO_2), nitrogen oxides (NO_X), and particulate matter (PM), impacting ecosystems and human health (Liu *et al*. 2023). Hence, the pressing need to efficiently transform corn residues into valuable commodities.

Pyrolysis is a widely utilized thermochemical conversion technology for biomass. It is recognized for its high efficiency in energy recovery. The primary products of biomass pyrolysis are bio-oil and biochar, both of which possess important value (Muigai *et al*. 2020). However, large-scale biomass applications necessitate an abundant supply of raw materials, often requiring the use of mixed biomass rather than a single biomass type (Defoort *et al*. 2019). Notable differences exist in the structure, composition, and physicochemical properties among various biomass feedstocks. Synergistic effects, whether positive or negative, may arise between different biomass components, potentially altering the activation energy and conversion kinetics during co-pyrolysis (Vyazovkin *et al*. 2014). Additionally, various pretreatment methods can modify the composition and structure of biomass, which profoundly impacts the pyrolysis process and noticeably influences the pyrolysis characteristics of mixed biomass, including kinetics, thermodynamics, reaction mechanisms, and product distribution (Suriapparao *et al*. 2018). Therefore, investigating these effects is essential for the design and optimization of the biomass co-pyrolysis process (Salema *et al*. 2019).

Alkaline pretreatment, particularly using NaOH, induces specific compositional and structural changes in lignocellulosic biomass. For corn residues, NaOH treatment primarily targets the removal of hemicellulose and lignin while preserving the cellulose framework (Haliman *et al*. 2025; Zhang *et al*. 2025a). During alkaline pretreatment, the hydroxide ions cleave the ether and ester bonds within lignin-carbohydrate complexes (LCCs), leading to the solubilization of lignin and partial hydrolysis of hemicellulose (Lin *et al*. 2024; Al Azad *et al*. 2025). Specifically, for corn cob and corn husk, NaOH treatment has been shown to significantly reduce hemicellulose and lignin contents while increasing the relative cellulose content (Haliman *et al*. 2025). The crystallinity index of cellulose typically decreases following NaOH treatment due to the transformation of cellulose I to cellulose II and the partial disruption of crystalline regions, which lowers the energy barrier for subsequent thermal decomposition (Wang *et al*. 2024). Furthermore, alkaline treatment induces morphological changes, including increased surface area and porosity, as the removal of amorphous components exposes the underlying cellulose microfibrils (Al Azad *et al*. 2025). These structural modifications enhance the pyrolytic reactivity of corn biomass by facilitating heat transfer and promoting dehydration reactions during the initial stages of pyrolysis (Ramírez-Estrada *et al*. 2024).

In recent years, substantial advances have been achieved in co-pyrolysis technologies, particularly concerning synergistic mechanisms, the catalytic effects of alkali and alkaline earth metals, and pretreatment strategies. These developments provide critical theoretical support for the efficient energy utilization of mixed biomass. Wei *et al*. (2025) systematically examined the staged pyrolysis behavior of acid-loaded corn cobs, clarifying the synergistic reaction mechanisms and the formation pathways of biofuel precursors. Chen (2025) conducted a comprehensive investigation into the co-pyrolysis behavior of various corn stalk tissues in conjunction with high-density polyethylene. This study revealed that the corncob/high-density polyethylene mixture yielded the highest amount of value-added chemicals and exhibited the lowest activation energy of 149.3 kJ/mol. Ma *et*

al. (2025a) implemented an alkaline-hydrogen peroxide synergistic pretreatment on sugarcane bagasse, demonstrating its effectiveness in disrupting the lignin-carbohydrate complex structure. This pretreatment increased the cellulose content from 30.6% to 75%. Following this treatment, the relative content of levoglucosan, a crucial product of cellulose fast pyrolysis, rose from 3.2% to 60.4%. Liu *et al*. (2025) examined the influence of alkali and alkaline earth metals (AAEMs) on the co-pyrolysis behavior of elm sawdust and coal through thermogravimetric analysis and a fixed-bed reactor. The results indicated that AAEMs demonstrated substantial catalytic activity, which lowered the pyrolysis temperature and maximum mass loss rate, facilitated the catalytic cracking of the organic matrix, and enhanced tar quality. Collectively, these findings provide a valuable reference for the corn cob-corn husk blends system employed in this study.

Current research on biomass co-pyrolysis has evolved from merely characterizing pyrolysis behavior to exploring multidimensional and interdisciplinary approaches, including pretreatment regulation and catalytic synergy. However, few studies have systematically investigated the mixed system of two typical agricultural residues, corn cob and corn husk, particularly for a 1:1 (wt%) cob-corn husk blend, with respect to the kinetics, reaction mechanisms, and product distribution under alkaline pretreatment. This study employed a corn cob-corn husk blend (1:1 wt%) to comparatively examine the co-pyrolysis behavior of raw and alkaline-pretreated samples. Thermogravimetric analysis, Pyrolysis-Gas Chromatography/Mass Spectrometry (Py-GC/MS), and various kinetic models were utilized to systematically assess the pyrolysis kinetics, thermodynamic parameters, and product distribution characteristics. This work aimed to elucidate the regulatory mechanisms of alkaline treatment on the co-pyrolysis characteristics of corn cob-corn husk blends, thereby providing a theoretical foundation and technical support for the efficient energy utilization of corn residue-based agricultural waste.

EXPERIMENTAL

Biomass Sample Preparation

Corn cob and corn husk utilized in this study were collected from a farm located in Zhengzhou, Henan Province, China. After washing and drying at 80 °C to constant weight, each material was individually ground and sieved through a 60 to 80 mesh. A blend of corn cob and husk was prepared in a ratio of 1:1 (w/w) based on the consideration of output matching, which was denoted as Sample A (SA). Subsequently, drawing on the research on alkali pretreatment of biomass (Tsegaye *et al*. 2019; Kim *et al*. 2025), SA was soaked in a 10 wt% NaOH solution for 2 h at a solid-to-liquid ratio of 1:10 (wt.%). After soaking, the sample was subjected to suction filtration, and the solid residue was repeatedly washed with distilled water until the washing solution tested neutral using pH test paper. The washed residue was then dried at 80 °C to a constant weight, yielding Sample B (SB). Finally, all the samples were kept in a desiccator.

Characterization of Blended Feedstocks

The proximate analysis of SA and SB was conducted on an as-received basis according to the method specified in Proximate analysis of solid biofuels (GB/T 28731-2012), and as-received basis fixed carbon content was calculated by mass difference. Elemental contents (C, H, N, S) were determined on a dry-basis using an elemental analyzer (Thermo Scientific FLASH 2000, USA). To calculate oxygen (O) content on a

dry basis, the as-received ash value was first converted to a dry basis using the moisture content. The dry-basis O was then calculated as: O (dry basis) = 100 − (C + H + N + S + Ash (dry basis)). The contents of cellulose, hemicellulose, and lignin in SA and SB were determined according to the standard analytical procedure developed by the National Renewable Energy Laboratory (NREL/TP-510-42618) (Sluiter *et al*. 2008). Fourier transform infrared (FTIR) analysis was performed to identify the functional groups of the samples. The samples were mixed with potassium bromide (KBr) powder at a ratio of 1:100 (w/w). The spectra were collected in the range of 4000 and 500 cm^{-1} (a resolution of 4 cm^{-1}, 32 scans) using a CT06484 FTIR spectrometer (PerkinElmer, American).

The powder X-ray diffraction (XRD) was used to determine the crystallinity index (CrI) of samples using a Bruker Rigaku TT Rax diffractometer (Rigaku TT Rax type, Bruker, Germany) with Cu-Kα radiation source (λ = 1.54 Å) operated at 40 kV and 40 mA. The XRD patterns were collected in the 2θ range of 5° to 90° at a scanning rate of 5°/min. CrI values were calculated using the following Eq. 1 (Segal *et al*. 1959),

$$\mathrm{CrI}(\%)=\left(\frac{I_{\mathrm{cry}}-I_{\mathrm{amp}}}{I_{\mathrm{cry}}}\right)\times 100 \quad (1)$$

where I_{cry} is the maximum diffraction intensity of crystalline region at $2\theta \approx 21.9°$ and I_{amp} is the minimum intensity corresponding to amorphous portion at $2\theta \approx 17.9°$.

Co-pyrolysis Analysis of Blended Samples

Thermogravimetric analysis

Thermogravimetric analysis was conducted with a TG209F3 thermogravimetric analyzer (Netzsch, Germany). A sample weighing approximately 7 to 9 mg was loaded into an alumina crucible and subjected to heating from 50 to 600 °C at rates of 10, 20, and 30 °C/min. During each run, high-purity nitrogen (99.99%) was passed through the TGA at a constant flow rate of 50 mL/min to provide the inert gas environment for pyrolysis and to sweep away the released volatile.

Co-pyrolysis products of the samples

To analyze the fast pyrolysis products of SA and SB, a Pyroprobe analytical pyrolyzer (Frontier-EGA/PY3030D, Japan) interfaced with a Shimadzu QP2010 Ultra GC/MS system was employed to differentiate and identify the pyrolytic volatiles. In each experiment, approximately 0.8 to 1 mg of sample was pyrolyzed at 550 °C for 30 s using high purity helium (99.99%) as the carrier gas. The volatiles products were separated by a chromatographic column (HP-5MS, 30 m × 0.25 mm × 0.25 μm), the GC oven temperature was programmed to hold at 50 °C for 2 min, then increased at 5 °C/min to 280 °C and hold for 10 min, and finally raised at 10 °C/min to 320 °C with a holding time of 10 min. The MS was operated from m/z 40 to 500 in an electron ionization (EI) mode at 70 eV. The volatile components were identified through the characteristic GC/MS spectra, which correlate with entries in the NIST MS database and references in published literature.

RESULTS AND DISCUSSION

Characterization of Raw Materials

Feedstock analysis

The elemental and proximate analysis results of the samples are summarized in Table 1. Previous studies have confirmed that feedstocks with a moisture content (MC) below 10 wt% are optimal for pyrolysis, as such a low moisture level facilitates efficient heat transfer and avoids adverse effects on pyrolysis efficiency caused by excessive moisture evaporation (Ahmad *et al*. 2017). The MC of SA and SB were 1.59 wt% and 2.01 wt%, which made them suitable for co-pyrolysis. Moreover, volatile matter (VM) and ash content (A) are widely recognized as the primary factors governing the yield of pyrolysis product, and A has been reported to be closely correlated with the calorific value of biomass (Vilas-Boas *et al*. 2024; Memon *et al*. 2026). Specifically, according to the findings of Waluyo *et al*. (2025), a high VM content endows biomass with superior volatility and reactivity, which is conducive to the formation and release of pyrolysis products. Conversely, low ash content is generally associated with a higher calorific value of the feedstock, as ash components (mainly inorganic minerals) do not contribute to energy release and may even catalyze undesirable side reactions during pyrolysis (Esteves *et al*. 2023). As presented in Table 1, the NaOH-treated blended sample exhibited a notable increase in volatile matter content, rising from 75.86 wt% to 84.27 wt%, while its ash content decreased substantially from 11.94 wt% to 1.88 wt%. These results further verify that the corn cob-husk mixture can serve as a promising feedstock for both pyrolysis and combustion processes. In particular, the SB sample treated with NaOH demonstrated exceptional suitability, because of its high volatile matter and low ash content.

Table 1. Proximate, Elemental and Component Analysis of the Samples

Analysis		Results	
		SA	SB
Proximate Analysis (wt%)	A	11.94	1.88
	MC	1.59	2.01
	VM	75.86	84.27
	FC	10.61	11.84
Elemental Analysis (wt%)	C	43.70	37.34
	H	5.85	5.38
	O	38.05	55.24
	N	0.27	0.12
	S	0.00	0.00
Component Analysis(wt%)	Cellulose	39.35	42.59
	Hemicellulose	26.18	20.78
	Lignin	8.62	2.54

*Proximate analysis is reported on an as-received basis (wt%), Elemental and Component analysis is reported on a dry basis (wt%).

Elemental analysis further corroborated the feedstock's practicality: SA contained 43.70 wt% C, 5.85 wt% H, 38.05 wt% O, 0.27 wt% N, and 0.00 wt% S. Both N and S contents were very low. Biomass feedstocks with low N and S are preferred for pyrolysis and combustion because they reduce the emissions of NOx and SOx (Yahya *et al*. 2023). After alkaline treatment (SB), the C content decreased to 37.34 wt%, while O increased to 55.24 wt%. This shift is consistent with the partial removal of lignin (C-rich, O-poor) and

relative enrichment of cellulose (C-poor, O-rich) (Stachowiak-Wencek *et al*. 2019). Compositional analysis confirms this interpretation: cellulose increased from 39.35 wt% (SA) to 42.59 wt% (SB), whereas hemicellulose and lignin decreased from 26.18 wt% and 8.62 wt% to 20.78 wt% and 2.54 wt%, respectively. Such changes are typical for alkaline pretreatment, which preferentially removes lignin and hemicellulose, leaving a cellulose-enriched solid residue (Kim *et al.* 2016). The ash content dropped sharply from 11.94 wt% (SA) to 1.88 wt% (SB), indicating effective demineralization by alkaline washing. Overall, the low N and S contents make both corn cob-husk blends promising alternative solid fuels for sustainable energy production.

XRD and FTIR analysis of the samples

The X-ray diffraction (XRD) patterns and Fourier-transform infrared (FTIR) spectra of SA and SB are presented in Fig. 1. As widely reported, biomass mainly comprises of cellulose and non-cellulose fractions (*i.e.*, hemicellulose and lignin) (Guida *et al*. 2021). As shown in Fig. 1 (a), SA exhibited two distinct diffraction peaks at approximately 16.3° and 21.9°, corresponding to the (110) and (200) plane diffractions of cellulose, respectively (Makhado *et al*. 2025). In contrast, SB displayed only one diffraction peak at around 20.6° with a slightly broadened width. This change in the diffraction pattern may be attributed to the alkali-induced polymorphic transformation of cellulose crystals (from cellulose I to cellulose II) and partial disruption of the crystal structure (Stanciu *et al*. 2025). Additionally, the alkali treatment may partially remove hemicellulose and lignin while retaining the cellulose framework (Hamid *et al*. 2023). According to Eq. 1, the crystallinity index (CrI) values of SA and SB were 30.1% and 19.3%, respectively, indicating a 10.8% decrease in crystallinity after alkali treatment. This reduction in crystallinity has direct implications for pyrolysis performance. Specifically, lower crystallinity promotes dehydration reactions in the cellulose solid matrix and facilitates the formation of oligosaccharides as reaction intermediates, ultimately increasing the yield of furans while decreasing levoglucosan production in the primary tar (Ma *et al*. 2025b). Furthermore, amorphous cellulose exhibits lower initial activation energy for pyrolysis compared to its crystalline counterpart, making it more readily decomposable (Yang *et al*. 2024; Ma *et al*. 2025b). The transformation of the cellulose crystal structure and partial disruption of crystalline regions thus lower the energy barrier required for cellulose thermal decomposition, thereby enhancing the pyrolytic reactivity of the alkali-treated biomass.

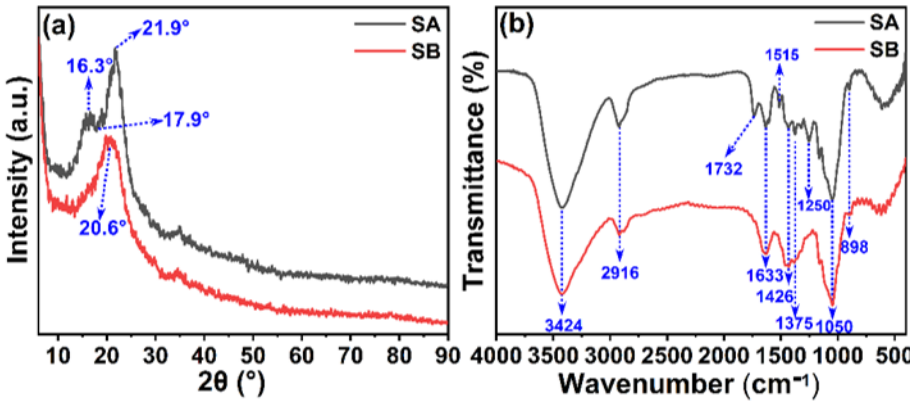

Fig. 1. XRD patterns (a) and FTIR spectra (b) of the samples

Fourier transform infrared (FTIR) spectroscopy was utilized for a preliminary analysis of the chemical structures of SA and SB, with the resulting transmittance spectra presented in Fig. 1 (b). The findings indicate noticeable structural alterations in the samples following alkali treatment. In the spectrum of SA, the broad band observed in the 3600 to 3200 cm^{-1} range, centered at 3424 cm^{-1}, is attributed to O-H vibrations of cellulose and intra- and intermolecular hydrogen bonds. The peak at 2916 cm^{-1} corresponds to C-H stretching vibrations of -CH_3 groups. The absorbance peaks at 1426 cm^{-1} and 1375 cm^{-1} are assigned to CH_2 bending vibrations in the crystalline region of cellulose and symmetric C-H deformation vibrations, respectively. The peak at 1250 cm^{-1} is associated with C-O stretching vibrations, while the characteristic peak at 898 cm^{-1} corresponds to the C_1-H deformation vibration of the *β*-glycosidic bond between glucose units, collectively confirming the presence of the cellulose skeleton (Woźniak *et al*. 2021). Additionally, the weak shoulder peak at 1732 cm^{-1} is attributed to C=O stretching vibrations of aliphatic esters in lignin and hemicellulose. The bands at 1633 cm^{-1} and 1515 cm^{-1} are assigned to C=C and C-C aromatic skeletal vibrations, respectively, originating from lignin. The absorbance peak at 1250 cm^{-1} is related to aromatic C-O stretching in guaiacyl and syringyl units, whereas the strong peak at 1050 cm^{-1} arises from C-O or C-O-C stretching vibrations. The comparison of the FTIR spectra of SA and SB indicates that the characteristic cellulose peaks (3424, 2916, 1426, 1375, 1050, and 898 cm^{-1}) in SB are preserved but exhibit diminished intensities. This observation suggests a partial disruption of the cellulose structure, while the main framework remains largely intact following alkali treatment (Pasca Supanta *et al*. 2025). In contrast, the characteristic peaks of lignin and hemicellulose (1732, 1633, 1515, and 1250 cm^{-1}) demonstrate a trend of either disappearance or attenuation, thereby confirming the effective removal of these components through alkali treatment (Awang *et al*. 2022; Sethi *et al*. 2024). These FTIR results align with the findings from XRD analysis.

The structural changes described above profoundly influence the distribution of pyrolysis products. The removal of hemicellulose and lignin, components that otherwise impede heat transfer during pyrolysis, combined with the reduced crystallinity of cellulose, enhances the pyrolytic reactivity of the biomass. More importantly, the residual sodium ions from alkali treatment act as catalytic active sites that promote cracking and reforming reactions during fast devolatilization, favoring the formation of gases (particularly CO_2) and char (Liu *et al*. 2025b; Wang *et al*. 2025c). The disappearance of lignin-related FTIR peaks also explains the reduced phenolic content in bio-oil from alkali-treated biomass, as lignin is the primary precursor of phenolic compounds during pyrolysis. These structure-performance correlations confirm that alkali treatment not only alters the physicochemical properties of the biomass but also fundamentally redirects the pyrolysis pathways toward gas and char formation at the expense of bio-oil yield (Liu *et al*. 2025b; Yang *et al*. 2024).

TGA analysis of the samples

The TG and DTG curves of SA and SB under pyrolysis conditions (50 to 600 °C, heating rates of 10, 20, and 30 °C/min) are presented in Fig. 2. The pyrolysis process of both samples can be categorized into three stages: stage I (dehydration stage), stage II (fast devolatilization stage), and stage III (carbonization stage). The first stage occurred at 50 to 220 °C for SA and 50 to 120 °C for SB, corresponding mass losses of 1.23 to 2.04 wt% and 1.99 to 2.79 wt%, respectively. Notably, the mass loss of SA and SB was essentially equivalent to their inherent moisture content (SA: 1.59 wt%, SB: 2.01%), indicating that this stage was primarily dominated by moisture removal. The DTG curves reveal that both

SA and SB displayed a minor peak at approximately 85 °C, with SB exhibiting a larger peak area compared to SA. This observation suggests an enhanced moisture removal rate following alkali treatment, likely due to the structural loosening of the biomass induced by the alkali treatment (Zheng *et al*. 2018).

In the second stage (220 to 420 °C), the DTG curve of SA displayed two distinct peaks at 304 to 310 °C and 339 to 355 °C, corresponding to the decomposition of hemicellulose and cellulose, respectively (Singh *et al*. 2021; Bilgin *et al*. 2025). These peaks were separated by a boundary temperature of approximately 325 °C, and the total mass loss in this stage amounted to 69.03 to 72.02 wt%. In contrast, the second stage for SB (120 to 360 °C) featured only a single DTG peak (282 to 300 °C) that shifted to a lower temperature. This difference is likely related to the partial removal of hemicellulose and the destruction of some cellulose structures following alkali treatment (Gong *et al*. 2022). The total mass loss for SB in this stage was 63.51 to 67.42 wt%. Regarding the third stage, SA (420 to 600 °C) shows a mass loss of 4.96 to 7.30 wt%, primarily due to lignin decomposition and aromatic ring polycondensation that forms biochar (Dong *et al*. 2024). SB, however, displayed a notably higher mass loss (10.52 to 10.85 wt%) in its third stage (360 to 600 °C). This increase suggests that beyond the decomposition of residual lignin, the degradation of cellulose II, generated during the alkali treatment, may be an additional contributing factor (Fengel *et al*. 1995; Zhang *et al*. 2023). The TG curves show that both samples stabilize after 530 °C, signaling the end of major pyrolysis reactions. The notably higher final residue yield of SB (32.57 to 36.49 wt%) compared to SA (20.98 to 24.44 wt%) underscores the advantage of alkali treatment for enhancing biochar production.

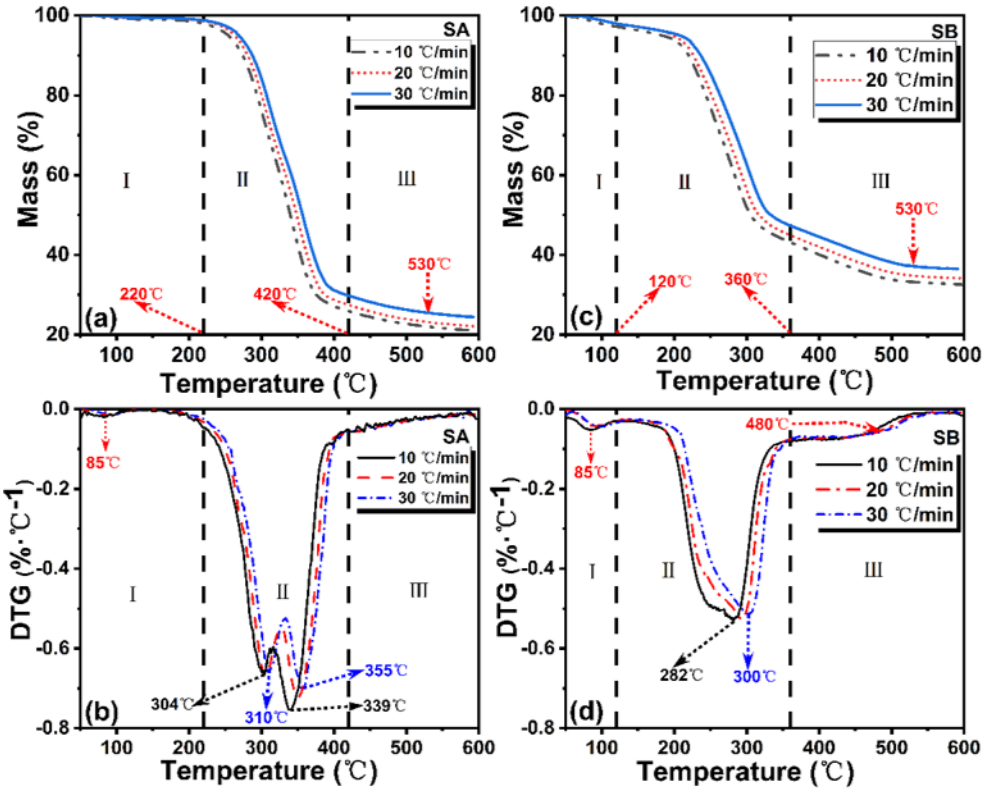

Fig. 2. TG (a, c) and DTG (b, d) curves *versus* temperature of the samples at heating rates of 10 °C/min, 20 °C/min, and 30 °C/min

Co-pyrolysis Kinetic Analysis

The kinetic parameters were derived from TG/DTG analysis of sample pyrolysis under a nitrogen atmosphere. As depicted in Fig. 2 (a) and (c), the TG curves at different heating rates reveal a pronounced dependence of the pyrolysis behavior on heating rate. With increasing heating rate, the curves gradually shifted towards high temperatures. However, the TG curves at different heating rates exhibited similar patterns, implying that the reaction mechanism of pyrolysis was not altered by the variation of heating rate, which validates the feasibility of employing these data for subsequent pyrolysis kinetic calculations (Rosu *et al*. 2018). The Kissinger-Akahira-Sunose (KAS) and Friedman (FR) methods, two widely adopted model-free approaches for solid-state reaction kinetics, were used to determine kinetic parameters (*i.e.*, activation energy E_α and pre-exponential factor A). With respect to SA, the DTG curves (Fig. 2) display two distinct mass loss rate peaks, which indicates that the pyrolysis process proceeds *via* two sequential decomposition reactions (Xia *et al*. 2022). To optimize the precision of subsequent kinetic calculations, the two mass loss stages (Zone I and Zone II) of SA were calculated separately, as shown in Fig. 3. The above-mentioned curves (α) *versus* temperature are presented in Fig. 4 (a) and (b). After alkaline treatment, the pyrolysis of SB was characterized by a single prominent weight loss rate peak (Fig. 2). The corresponding α *versus* temperature curves are also plotted, which is shown in Fig. 4 (c).

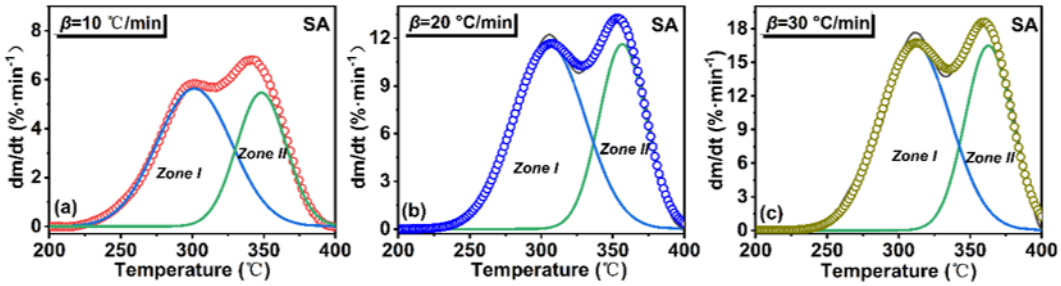

Fig. 3. dm/dt curves *versus* temperature of SA at heating rates of 10 °C/min(a), 20 °C/min(b), and 30 °C/min(c)

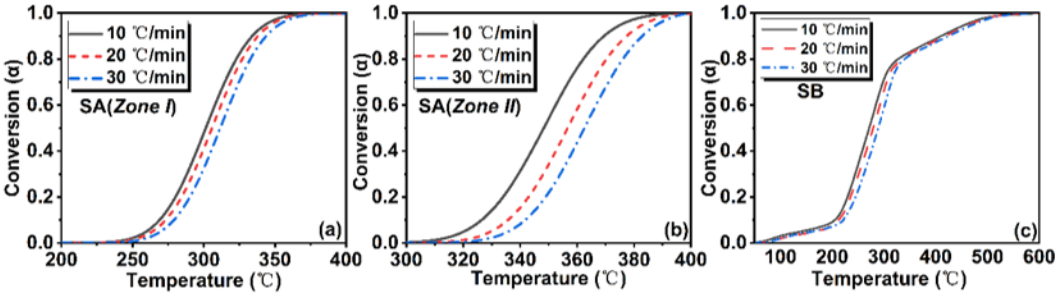

Fig. 4. Conversion curves *versus* temperature of SA in Zone Ⅰ (a), Zone Ⅱ (b), and SB (c) at heating rates of 10 °C/min, 20 °C/min, and 30 °C/min

The relationships between $\ln(\beta \cdot d\alpha/dT)$ and $1000/T$ for the Friedman (FR) method, and $\ln(\beta/T^2)$ and $1000/T$ for the Kissinger-Akahira-Sunose (KAS) method, are presented in Fig. 5. All fitted lines achieved correlation coefficients (R^2) exceeding 0.97 over the conversions range of 0.2 to 0.8, indicating the reliability of linear fitting. From these plots in Fig. 5, the relationship between the E_α and α was determined, as shown in Fig. 6. As evidenced in this figure, E_α values were not analogous at different conversion rate, because

most solid-state reaction mechanisms tend to have a complex multi-step reaction (Pitchai *et al*. 2019). The average E_α values determined *via* the KAS and FR methods ranged from 288.58 to 299.71 kJ/mol for SA in Zone I, 242.10 to 261.53 kJ/mol for SA in Zone II, and 161.67 to 176.85 kJ/mol for SB in pyrolysis process. It is apparent from Fig. 6 that E_α values increased with the α increasing from 0.2 to 0.8. At initial conversion (α = 0.2), the activation E_α values was relatively low, which may be attributed to the decomposition of hemicellulose and the amorphous regions of cellulose in the early stages of biomass pyrolysis, as these components have weaker chemical structures that require less energy to break. As the α increased, stronger bonds within the biomass began to participate in the reaction, requiring higher activation energy to decompose these more stable molecules. Compared with SA, a distinct evolution pattern of E_α was observed for SB. For SA (Zone I) and SA (Zone II), E_α increased linearly with α. For SB, E_α remained at a relatively low level when α was below 0.6, but increased sharply once α exceeded 0.7, eventually reaching a final E_α value at α = 0.8 comparable to that of SA. This variation in E_α is associated with the partial destruction of the cellulose structure and the removal of lignin caused by alkali treatment (Wang *et al*. 2025a). Overall, the lower average E_α for SB compared to SA demonstrates its enhanced thermodynamic favorability for pyrolysis. This finding further indicates that alkali treatment can serve as an effective pretreatment method to promote biomass pyrolysis by lowering the energy barrier of the reaction system.

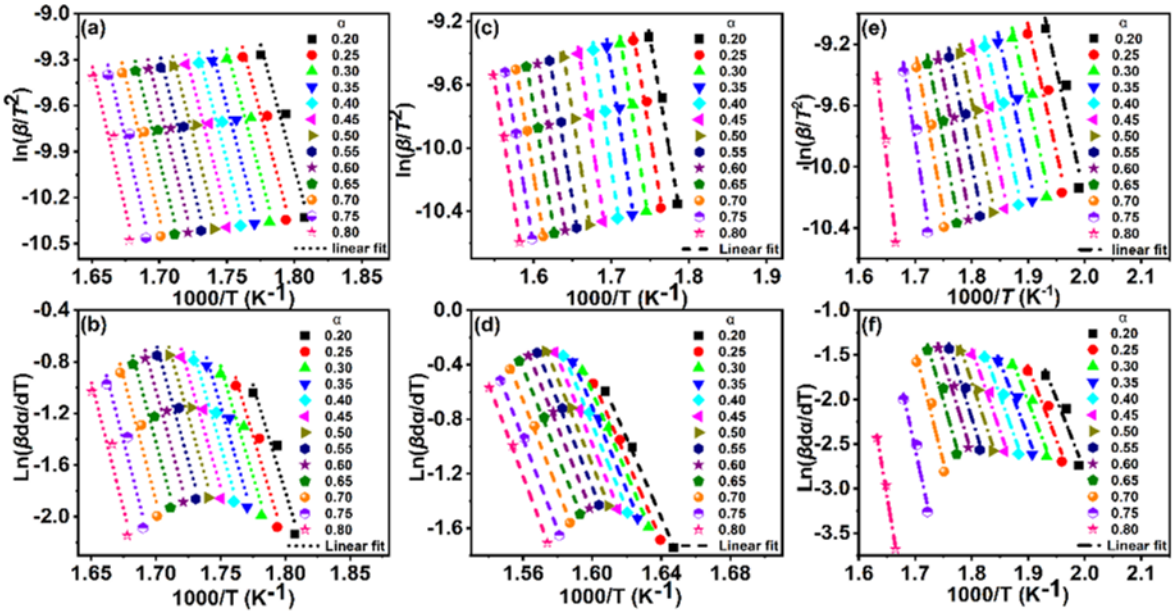

Fig. 5. Plots of ln(*β*·dα/dT) *vs.*1000/*T* and ln(*β*/*T*) *vs.* 1000/*T* by methods of KAS and FR of (a, b) SA (Zone I), (c, d) SA (Zone II) and (e, f) SB

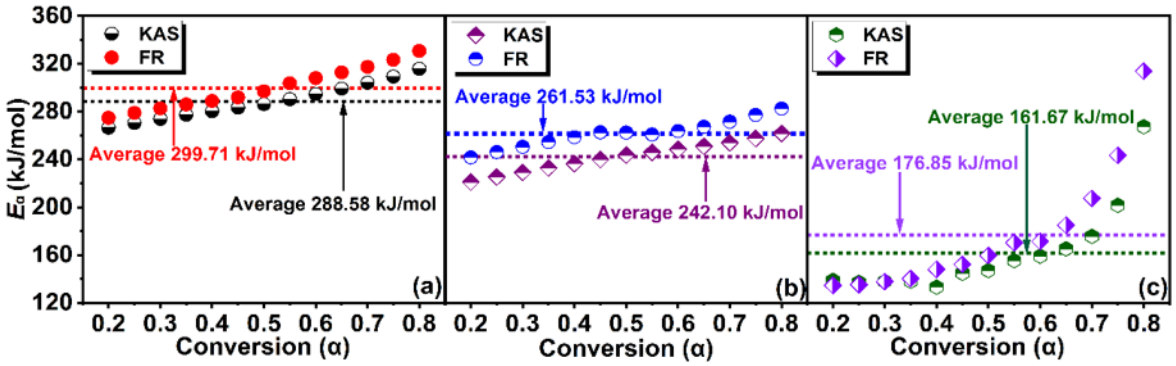

Fig. 6. The activation energy (E_α, kJ/mol) of SA (Zone I) (a), SA (Zone II) (b), and SB (c) calculated using the KAS and FR methods

Co-pyrolysis Mechanism Analysis

The pyrolysis mechanism of the samples was studied by the method proposed by Criado *et al*. (1989) at a heating rate of 10 °C/min. Figure 7 shows the theoretical and experimental curves for the pyrolysis process of the samples. The theoretical curves for models ranging from nucleation and growth (A2) to random nucleation with three nuclei on the individual particle (F3) were obtained from the solid-state models (Wang *et al*. 2025a). Table S1 presents the functional expressions of the most common reaction mechanisms in solid reactions. The experimental curves (Z(a)-SB, Z(a)-SA (Zone I), and Z(a)-SA (Zone II)) were plotted using E_α calculated by the FR method. The pyrolysis mechanism of the samples were subsequently identified by comparing the fitting degree between theoretical curves and the experimental curves.

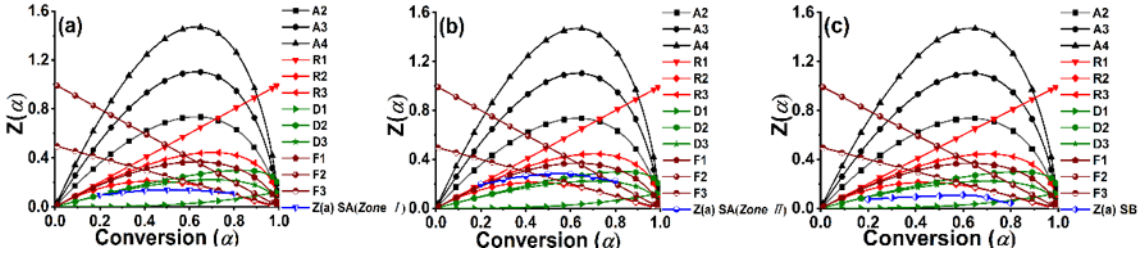

Fig. 7. Theoretical curves and experimental values obtained using the Criado method for SA (Zone I) (a), SA (Zone II) (b), and SB (c)

Analysis of the kinetic mechanism function revealed notable disparities in the reaction control mechanisms among the samples. As depicted in Fig. 7, the experimental curve of SA (Zone II) generally agreed with the theoretical curve of the random nucleation with one nucleus on the individual particle (F1) mechanism (n = 1), indicating that random nucleation and subsequent nuclear growth govern the pyrolysis in this phase. Conversely, the experimental curves of SB and SA (Zone I) resembled each other and aligned well with the theoretical curve of the three-dimensional diffusion model (D3) mechanism (Jander equation, n = 2), suggesting that their pyrolysis processes were predominantly regulated by the three-dimensional diffusion of volatiles through the solid product layer. Following alkali treatment, the reaction mechanism of SB shifted from a combination of multiple mechanisms to a singular mechanism predominantly controlled by diffusion. This consolidation of the mechanism helps to enhance the controllability and efficiency of the

pyrolysis process (Zhang *et al*. 2025b). The influence of alkali treatment on the reaction mechanism can be attributed to the partial disruption of the cellulose structure and the partial elimination of hemicellulose and lignin (Ellison *et al*. 2023). These structural alterations diminish the mass transfer resistance within the system, consequently leading to a pyrolysis process more inclined to be governed by the diffusion step.

Thermodynamic Parameter Analysis

The pre-exponential factor (A) was determined using E_α values derived from the FR method at a heating rate of 10 °C/min, as detailed in Table 2. A crucial kinetic parameter, the A value characterizes pyrolysis behavior and is influenced by biomass composition and the intricate reactions during pyrolysis. As per transition state theory, the A value is directly proportional to the activation entropy (ΔS). Lower A values typically signify systems with limited reactivity and tightly bound complexes, while higher A values indicate increased activation entropy, implying heightened reactivity and a less constrained transition state structure (Vyazovkin 2024). In this study, the A values for SA (Zone I and Zone II) increased linearly with the conversion degree α from 0.2 to 0.8, ranging from 1.2×10^{23} to 1.7×10^{28} s^{-1} and from 5.5×10^{18} to 1.9×10^{22} s^{-1}, respectively. The broad distribution and continuous evolution of A values indicate that the pyrolysis of SA involves multiple mechanisms synergistically, with the reaction pathway dynamically evolving as conversion progresses. In contrast, SB displayed a stage-dependent behavior in its A values. For α below 0.6, the A values remained relatively low and stable, within the range of 10^{10} to 10^{14} s^{-1}. This behavior can be attributed to two competing factors. On one hand, the NaOH pretreatment removes a substantial portion of intrinsic AAEMs (*e.g.*, K, Ca, Mg) from the raw biomass, which suppresses catalytic side reactions in the initial stages and simplifies the reaction pathway in the primary reaction zone (Wang *et al*. 2025b; Li *et al*. 2025). On the other hand, residual sodium ions from the NaOH treatment itself remain in the sample even after washing. These residual Na species can act as catalytic active sites during pyrolysis (Liu *et al*. 2025; Wang *et al*. 2022). Notably, the relatively low and stable A values in the early stage ($\alpha < 0.6$) suggest that the removal of intrinsic AAEMs dominates the catalytic effect during primary devolatilization, while the catalytic contribution of residual Na becomes more pronounced in the later stages. This interpretation is consistent with recent findings that Na exhibits the highest catalytic cracking activity among AAEMs, effectively stabilizing alkyl radicals and promoting decarboxylation reactions (Ting *et al*. 2020; Wang *et al*. 2022).

However, when α exceeded 0.7, the A value increased sharply to the range of 10^{17} –10^{25} s^{-1}. This abrupt transition marks a clear shift from depolymerization reactions dominating the primary reaction zone to complex polycondensation and carbonization reactions in the later stages. Residual sodium ions retained from the alkali treatment are likely to catalyze these condensation reactions, thereby contributing to the sharp rise in A values. This stage-dependent behavior indicates that although alkali treatment simplifies the reaction pathway in the main pyrolysis zone, it does not eliminate the inherent complexity of subsequent stages. Instead, the introduction of exogenous sodium *via* NaOH treatment introduces its own catalytic effects, particularly in promoting char-forming condensation reactions at high conversion degrees. This dual role of both removing inherent AAEMs and introducing residual sodium offers a theoretical foundation for understanding the pyrolysis mechanism of alkali-treated biomass and achieving targeted regulation of pyrolysis products (Vyazovkin *et al*. 2011; Yu *et al*. 2025).

Beyond the kinetic triplet parameters (E_α, A, and $f(\alpha)$), thermodynamic parameters (ΔG, ΔH, and ΔS) are also essential for understanding and optimizing the biomass pyrolysis process. These thermodynamic parameters were calculated using E_α and A values derived from the FR method, with the results shown in Fig. 8. In biomass pyrolysis, ΔG reflects the energy input required for the reaction process. A higher ΔG value indicates a greater energy requirement for the pyrolysis process, whereas a lower ΔG value suggests lower energy consumption for generating pyrolysis products. As shown in Fig. 8 (a), (d), and (g), the average ΔG values calculated *via* FR for SA (Zone I), SA (Zone II), and SB across the entire conversion process were 160.77, 175.15, and 160.01 kJ/mol, respectively. The increase of conversion (0.2 to 0.8) exerted no noticeable influence on the ΔG values, indicating that the thermodynamic energy barrier remained relatively stable during the main pyrolysis stage. Notably, the average ΔG value of SA (Zone II) was higher than those of SA (Zone I) and SB, a phenomenon that may be attributed to the pyrolysis characteristics of cellulose and lignin components (Sankhla *et al*. 2025).

Table 2. Pre-exponential Factors (A, s^{-1}) of SA and SB *via* FR

Conversion (α)	A/s^{-1}		
	SA-Zone Ⅰ	SA-Zone Ⅱ	SB
0.20	1.2×10^{23}	5.5×10^{18}	4.1×10^{10}
0.25	3.0×10^{23}	1.3×10^{19}	4.7×10^{10}
0.30	6.6×10^{23}	3.2×10^{19}	8.0×10^{10}
0.35	1.3×10^{24}	7.2×10^{19}	1.4×10^{11}
0.40	2.4×10^{24}	1.6×10^{20}	8.1×10^{11}
0.45	4.6×10^{24}	3.7×10^{20}	2.1×10^{12}
0.50	1.4×10^{25}	3.5×10^{20}	1.1×10^{13}
0.55	5.6×10^{25}	2.6×10^{20}	1.2×10^{14}
0.60	1.4×10^{26}	4.5×10^{20}	1.5×10^{14}
0.65	3.8×10^{26}	9.1×10^{20}	3.1×10^{15}
0.70	1.0×10^{27}	2.2×10^{21}	4.5×10^{17}
0.75	3.6×10^{27}	6.6×10^{21}	1.3×10^{21}
0.80	1.7×10^{28}	1.9×10^{22}	6.8×10^{27}
Mean value	1.7×10^{27}	2.4×10^{21}	5.3×10^{26}

The ΔH term corresponds to the total thermal energy consumed in generating value-added products. The ΔH values for all samples were positive across the conversion range of 0.2 to 0.8, confirming that the pyrolysis process is endothermic. As shown in Fig. 8 (b), (e), and (h), the ΔH values gradually increase with α, indicating that the thermal energy required increases as the pyrolysis reaction progresses, which may be attributed to the involvement of lignin during the later stages of pyrolysis. Furthermore, throughout the pyrolysis process, the average differences between ΔH and E_α for SA (Zone I), SA (Zone II), and SB were calculated to be approximately 4.8, 5.2, and 4.7 kJ/mol, respectively. This minor difference suggests that the activation energy required for generating pyrolysis products was only slightly higher than the total thermal energy absorbed by the reaction, implying a relatively low reaction energy barrier. From an energy perspective, this pyrolysis process is thermodynamically favorable to initiate (Wang *et al*. 2025c). ΔS

reflects the degree of disorder within the pyrolysis system. A higher Δ*S* value indicates a greater deviation from thermodynamic equilibrium and enhanced reactivity, whereas a lower Δ*S* value suggests reduced reactivity (Sankhla *et al*. 2023). The Δ*S* values for both SA (Zone I) and SA (Zone II) were positive and increased with *α*, indicating a continuous rise in the disorder of the system throughout the pyrolysis process. In contrast, the Δ*S* of SB exhibited stage-dependent characteristics. When $\alpha < 0.55$, Δ*S* was negative, implying that the activated complex formed at this stage possessed a higher molecular order compared to the original biomass structure (Salami *et al*. 2025). However, when $\alpha > 0.55$, Δ*S* became positive, indicating an increase in system disorder at high conversion rates and an enhancement in the kinetic favorability of the pyrolysis reaction.

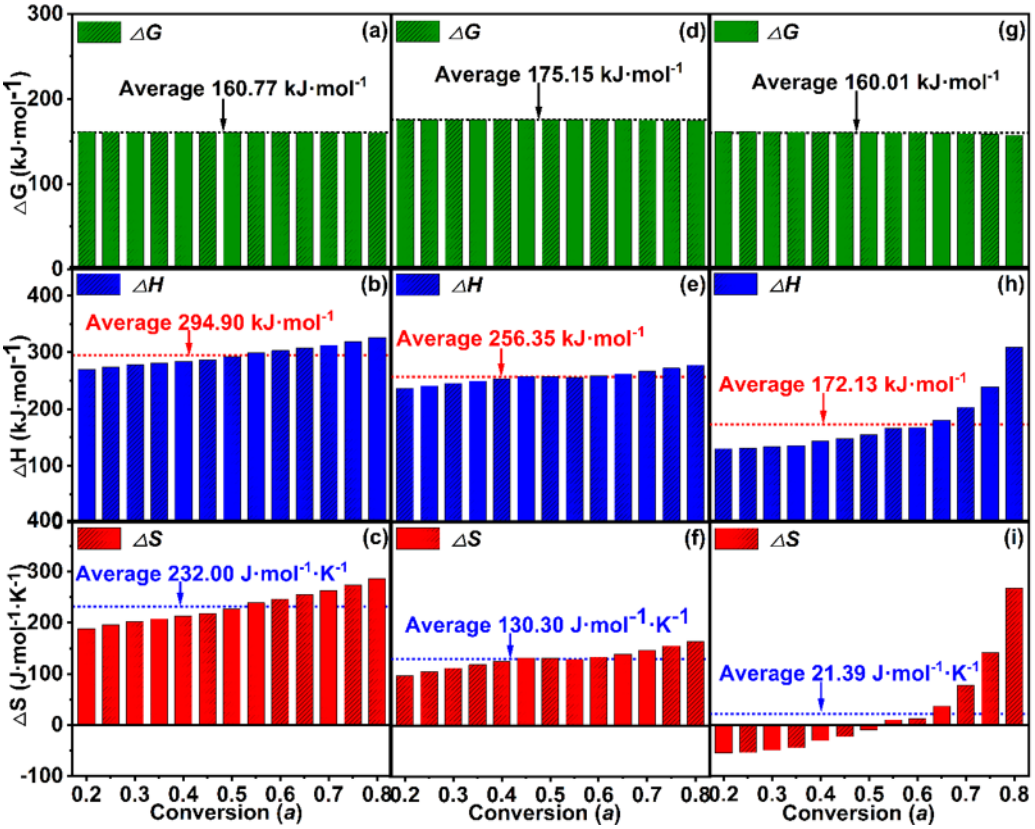

Fig. 8. Thermodynamic parameters (Δ*G*, Δ*H*, and Δ*S*) of SA (Zone I) (a, b, c), SA (Zone II) (d, e, f), and SB (g, h, i) at various conversions

Co-pyrolysis Product Analysis

To accurately analyze the pyrolysis products of the samples, Py-GC/MS was conducted. The resulting mass spectra were matched against the National Institute of Standards and Technology (NIST) library to identify individual compounds, which are detailed in Table 3. The chemical structures of the identified compounds are presented in Table S2. Figure 9 presents the gas chromatography-mass spectrometry (GC-MS) chromatograms of the pyrolytic products. Based on their characteristic functional groups, the identified compounds were categorized into carbonyls, phenolics, aliphatics, aromatics, and heterocyclic compounds, as illustrated in Fig. 10 (a). As one of the predominant pyrolytic fractions, carbonyl compounds accounted for 23.27% and 17.99% of the total detected products for SA and SB, respectively. This group was primarily comprised of aldehydes, ketones, and acids. Specifically, acids are predominantly generated from the

cleavage of O-acetyl groups inherent in hemicellulosic polysaccharide units. Aldehydes are formed *via* the *β*-scission of cellulose monomer molecules, while ketones are mainly produced through the intramolecular ketonization of acids following dehydration (Ellison *et al*. 2023). Notably, a high acid content in bio-oil is generally associated with corrosiveness and instability, which can compromise its quality. The alkali pretreatment substantially removed hemicellulose from SB, thereby reducing acid formation during pyrolysis and contributing to an improvement in bio-oil quality. Phenolic compounds represent another critical category of pyrolysis products, primarily derived from the cleavage of aryl ether linkages (*e.g.*, *α*-O-4, *β*-O-4) and carbon-carbon bonds (*e.g.*, *β*-5) in lignin (Lu and Gu 2022). As depicted in Fig. 10, the yield of phenolic compounds from SB (3.6%) was noticeably lower than that from SA (15.47%). This discrepancy is attributed to the partial delignification of SB during the alkali pretreatment. The identified aliphatic compounds accounted for 10.78% and 4.22% of the total products for SA and SB, respectively. These compounds most likely originated from the conversion of cellulose to levoglucosan *via* glycosidic bond cleavage, followed by further fragmentation of levoglucosan. Aromatic compounds, comprising 9.00% (SA) and 1.72% (SB) of the products, were likely generated from the decomposition of aromatic polymers at elevated temperatures, a process primarily caused by lignin degradation (Ma *et al*. 2022). Furthermore, heterocyclic compounds were detected, with relative contents of approximately 3.01% for SA and 1.85% for SB. These can be broadly classified into nitrogen-containing and oxygen-containing heterocycles. Nitrogen-containing heterocycles, which are valuable building blocks in pharmaceuticals and fine chemicals, are predominantly formed through deamination, cyclization, and condensation reactions of nitrogenous organic components (*e.g.*, proteins and amino acids) present in the feedstock during pyrolysis (Yuan *et al*. 2018). In contrast, oxygen-containing heterocycles are mainly generated *via* ring-opening, dehydration, and rearrangement reactions of cellulose and hemicellulose (Yunpu *et al*. 2018). The resulting pyrolytic products hold potential as both precursors for organic chemical synthesis and as biomass-derived fuels for power generation and heating.

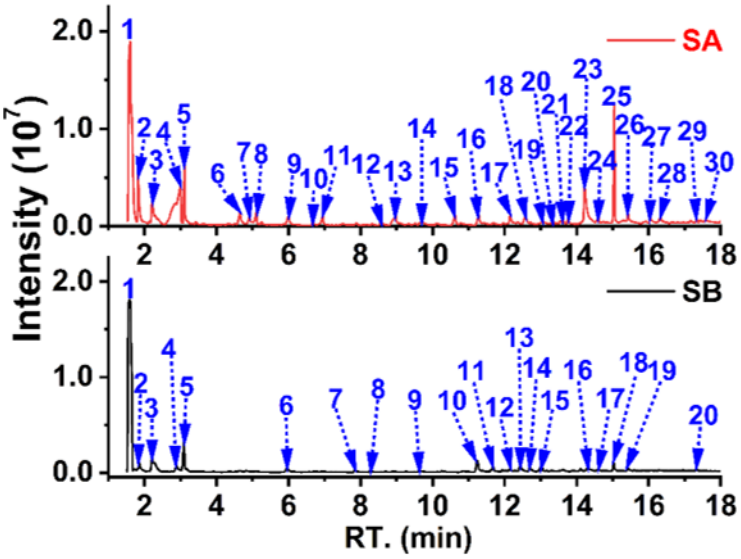

Fig. 9. GC-MS chromatogram of the pyrolysis compositions of samples. Key compounds are marked on the peaks, and the detailed peak identification is provided in Table 3 according to the labeled numbers

Table 3. Pyrolysis Compositions of Samples Obtained from Py-GC/MS at 550 °C

Sample	No.	RT. (min)	Component	Area (%)
SA	1	1.6	Carbon dioxide	38.47
	2	1.8	n-Butane	6.41
	3	2.2	2,3-Butanedione	2.75
	4	2.9	Acetic acid	6.88
	5	3.1	Hydroxyacetone	3.87
	6	4.7	Methyl pyruvate	2.05
	7	4.9	Succindialdehyde	1.21
	8	5.1	Ethyl pyruvate	1.74
	9	6.0	4,5-Dimethylimidazole	1.24
	10	6.7	3-Methyl-2-heptanone	0.49
	11	7.0	1-(acetyloxy)-2-Propanone	1.51
	12	8.6	2(5H)-Furanone	0.42
	13	9.0	Cyclohexanone	2.30
	14	9.7	7-Oxabicyclo[2.2.1]heptan-2-one	1.23
	15	10.6	cis-1,2-Dihydrocatechol	1.46
	16	11.3	Cyclooctane	1.59
	17	12.2	2-methoxy-Phenol	1.79
	18	12.6	Cyclopropyl carbinol	1.54
	19	13.1	3,6-Dimethyl-tetrahydropyran-2-one	0.92
	20	13.3	dihydro-2H-Pyran-3(4H)-one	0.43
	21	13.5	2-ethyl-Phenol	0.33
	22	13.8	1-Methylhexyl hydroperoxide	0.48
	23	14.2	Phenoxyethene	7.39
	24	14.6	4-ethyl-2-methoxy-Phenol	0.31
	25	15.0	4-vinyl-2-methoxy-Phenol	7.22
	26	15.4	2,4-Dimethoxyphenol	1.24
	27	16.0	4-Hydroxy-2-methoxybenaldehyde	1.05
	28	16.3	2-methoxy-4-propenyl-Phenol	1.58
	29	17.3	4-(3-hydroxy-1-propenyl)-2-methoxy-Phenol	0.56
	30	17.6	4-allyl-2,6-dimethoxy-Phenol	1.54
SB	1	1.6	Carbon dioxide	70.61
	2	1.9	n-Butane	2.59
	3	2.2	2,3-Butanedione	2.69
	4	2.9	2-Oxopropanoic acid	2.33
	5	3.1	Hydroxyacetone	5.59
	6	6.0	3,4-Dimethyl-1H-pyrazole	1.48
	7	7.8	2-Methyl-2-cyclopentenone	0.68
	8	8.3	Butyrolactone	0.37
	9	9.6	2-Methyl-2-cyclopentenone	0.40
	10	11.3	3-Methylcyclopentane-1,2-dione	3.45
	11	11.7	(Z)-2-Undecene	1.03
	12	12.2	2-methoxy-Phenol	0.75
	13	12.4	Cyclopropyl carbinol	2.00
	14	12.7	4-Ethylcyclohexanone	0.87
	15	13.0	2-Methylenecyclohexanol	0.61
	16	14.3	(Ethenyloxy)-Benzene	1.22
	17	14.6	4-ethyl-2-methoxy-Phenol	0.33
	18	15.0	2-Methoxy-4-vinylphenol	1.64
	19	15.4	2,4-Dimethoxyphenol	0.89
	20	17.3	4-(3-hydroxy-1-propenyl)-2-methoxy-Phenol	0.50

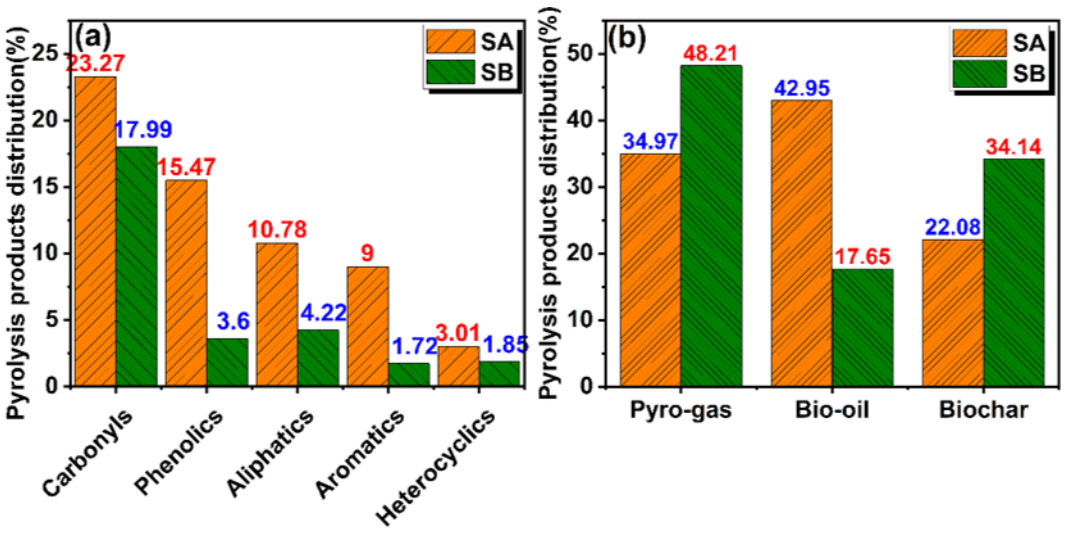

Fig. 10. Pyrolysis products classification of samples according to composition (a) and phase (b) at 550 °C

The three-phase product distribution obtained by Py-GC/MS analysis is shown in Figure 10(b). For SA, the yields of pyro-gas, bio-oil, and biochar were 34.97%, 42.95%, and 22.08%, respectively. After alkali pretreatment, the pyro-gas yield increased to 48.21% (with carbon dioxide as the dominant component), the biochar yield rose to 34.14%, while the bio-oil yield decreased to 17.65%. These changes were not merely differences in data but rather reflected differences in the mechanism of action induced by alkali pretreatment, a pattern consistent with the conclusions of recent related studies (Song and Lee 2024; Liu *et al*. 2025; Wang *et al.* 2025c).

The increase in biochar yield is attributed to several factors. First, alkali pretreatment promotes the partial removal of amorphous components (such as hemicellulose and lignin), thereby increasing the relative content of cellulose. During pyrolysis, crystalline cellulose is more inclined to undergo carbonization reactions through synergistic dehydration and crosslinking pathways (Ellison *et al.* 2023). Second, alkali treatment induces structural crosslinking between lignin and carbohydrate components, forming a more thermally stable lignin-carbohydrate complex, which is directly converted into biochar and increases the biochar yield (Song and Lee 2024). Third, the residual sodium ions in the biomass after alkali pretreatment can act as catalytic active sites, which not only facilitate the catalytic cracking of the organic matrix but also enhance biochar yield by stabilizing alkyl radicals (Liu *et al.* 2025; Wang *et al*. 2025c). Conversely, the decrease in bio-oil yield is due to, on one hand, the removal of alkali-soluble extracts and part of the lignin by sodium hydroxide pretreatment, substances that would otherwise decompose to generate phenolic-rich bio-oil components. On the other hand, during pyrolysis, residual sodium ions catalyze the cracking and reforming of bio-oil precursors (such as levoglucosan, furans, and phenolic compounds) into small-molecule non-condensable gases, primarily carbon dioxide (Liu *et al*. 2025); the significant increase in carbon dioxide yield also confirms this process.

In summary, alkali pretreatment was found to exert a bidirectional regulatory effect on product distribution: it promoted biochar formation through structural crosslinking and alkali-catalyzed repolymerization, while reducing bio-oil yield *via* catalytic cracking (especially decarboxylation reactions) and char-forming competitive reactions. The

findings indicate that alkali pretreatment favored an increase in biochar yield and was able to selectively improve bio-oil quality (*e.g.*, by reducing oxygen content and acidity (Ellison *et al.* 2023)), albeit at the expense of bio-oil yield.

CONCLUSIONS

1. The pyrolysis products of untreated blends of corn cob and corn husk (SA) and corresponding blends pretreated with 10% NaOH (SB) contained quantities of valuable organic compounds, such as carbonyl compounds, phenols, heterocyclic compounds, aromatics, and aliphatic compounds, as well as biochar, representing 42.95% and 17.65% of the total pyrolysis products of SA and SB, respectively. The biochar contents were 22.08% and 34.14%, respectively, suggesting the potential for high-value utilization of both materials.
2. Kinetic analysis indicated that the average E_α of SA ranged from 288.58 to 299.71 kJ/mol in Zone I and from 242.10 to 261.53 kJ/mol in Zone II. In contrast, the average E_α of SB throughout the pyrolysis process was between 161.67 and 176.85 kJ/mol, suggesting that NaOH treatment effectively lowered the E_α. The A value for SA increased linearly with the conversion rate (α = 0.2 to 0.8), varying from 1.2×10^{23} to 1.7×10^{28} s^{-1} in Zone I and from 5.5×10^{18} to 1.9×10^{22} s^{-1} in Zone II, demonstrating a broad continuous distribution. For SB, the A value exhibited a staged variation, remaining stable at 10^{10} to 10^{14} s^{-1} when α was below 0.6, and then sharply increasing to 10^{17} to 10^{25} s^{-1} when α exceeded 0.7.
3. Thermodynamic analysis indicated that the difference between E_α and ΔH for SB was approximately 4.7 kJ/mol, which was marginally lower than that for SA. For SA, this difference was approximately 4.8 kJ/mol in Zone I and about 5.2 kJ/mol in Zone II.
4. As the pyrolysis temperature increased, the pyrolysis mechanism of SA shifted from a three-dimensional diffusion model (D3) in Zone I to a random nucleation model (F1) in Zone II. In contrast, SB adhered to the three-dimensional diffusion model (D3) consistently throughout the entire pyrolysis process.
5. The NaOH treatment greatly influenced the pyrolysis process of corn cob-husk blends. From the perspectives of kinetic and thermodynamic analyses, it facilitated this process. In terms of the pyrolysis mechanism, the treatment transitions the mechanism from a combination of multiple mechanisms to a single diffusion-controlled mechanism, thereby enhancing both the controllability and efficiency of pyrolysis. Regarding product distribution, although NaOH treatment suppressed bio-oil yield, it effectively promoted biochar formation. Consequently, the pyrolysis of SA is advantageous for bio-oil production, while that of SB favors biochar formation, thus providing a foundation for the high-value utilization of corn cob-husk blends.

ACKNOWLEDGMENTS

This work was supported by the construct program of the key discipline in Zhengzhou University of Technology, Higher Education Teaching Reform Research and Practice Project of Henan Province (No. 2024SJGLX0565, 2026SJGLX617), Henan

Province Characteristic Demonstration Course on Integration of Specialty and Innovation: Chemical Technology (JiaoBanGao [2024]144, NO.168), Henan Province Undergraduate University Industry-Education Integration Project (JiaoBanGao [2024]13, NO.50), Henan Province Key Scientific Research Projects in Higher Education Institutions (No. 26B430029, 26B430028), College Students' Innovation and Entrepreneurship Training Program of Henan Province (No. S202511068017, S202511068021, S202511068024), and the Natural Science Foundation of Henan Province (No. 252300420497).

REFERENCES CITED

Ahmad, M. S., Mehmood, M. A., Al Ayed, O. S., Ye, G., Luo, H., Ibrahim, M., Rashid, U., Nehdi, I. A., and Qadir, G. (2017). "Kinetic analyses and pyrolytic behaviour of Para grass (*Urochloa mutica*) for its bioenergy potential," *Bioresource Technology* 224, 708-713. https://doi.org/10.1016/j.biortech.2016.10.090

Al Azad, S., Madadi, M., Rahman, A., Sun, C., Zhang, E., and Sun, F. (2025). "Quantum mechanical insights into lignocellulosic biomass fractionation through an NaOH-catalyzed Triton-x 100 system: In vitro and in silico approaches," *ACS Sustainable Chemistry & Engineering* 13(15), 5516-5530. https://doi.org/10.1021/acssuschemeng.4c09654

Awang, N. A., Salleh, W. N. W., Ismail, A. F., Aziz, F., and Yusof, N. (2022). "Structural characterization of acid and alkali treated-corncob waste: A potential resources biosorbent," in: *AIP Conference Proceedings* 2610(1), article 020004. https://doi.org/10.1063/5.0100099

Bilgin, S., Yılmaz, H., Topakcı, M., Gürdil, G. A. K., Çanakcı, M., and Karayel, D. (2025). "Determination of the pyrolytic characteristics of various biomass pellets," *Sustainability* 17(20), article 9003. https://doi.org/10.1016/j.joei.2017.06.002

Chen, B. (2025). *Thermal Processing of Agricultural Waste-based Biorefinery Residues and Plastics for Producing Sustainable Fuels and End of Life Value*, Doctoral Dissertation, University of Glasgow, Glasgow, UK.

Criado, J. M., Malek, J., and Ortega, A. (1989). "Applicability of the master plots in kinetic analysis of non-isothermal data," *Thermochimica Acta* 147(2), 377-385. https://doi.org/10.1016/0040-6031(89)85192-5

Defoort, F., Campargue, M., Ratel, G., Miller, H., and Dupont, C. (2019). "Physico-chemical approach to blend biomass," *Energy & Fuels* 33(7), 5820-5828. https://doi.org/10.1021/acs.energyfuels.8b04169

Dong, Z., Yang, H., Laine, R., Leclerc, S., Chen, L., Hua, D., and Chen, H. (2024). "A comprehensive *in-situ* analysis of lignin softening and pyrolysis mechanism," *Proceedings of the Combustion Institute* 40(1-4), article 105603. https://doi.org/10.1016/j.proci.2024.105603

Ellison, C., Garcia-Perez, M., Mullen, C. A., and Yadav, M. P. (2023). "Thermochemical behavior of alkali pretreated biomass – A thermogravimetric and Py-GC/FID study," *Sustainable Energy & Fuels* 7(14), 3306-3315. https://doi.org/10.1039/D3SE00213F

Enawgaw, H., Tesfaye, T., Yilma, K. T., and Limeneh, D. Y. (2023). "Multiple utilization ways of corn by-products for biomaterial production with bio-refinery concept; a review," *Materials Circular Economy* 5(1), article 7. https://doi.org/10.1007/s42824-023-00078-6

Esteves, B., Sen, U., and Pereira, H. (2023). "Influence of chemical composition on heating value of biomass: A review and bibliometric analysis," *Energies* 16(10), article 4226. https://doi.org/10.3390/en16104226

Fengel, D., Jakob, H., and Strobel, C. (1995). "Influence of the alkali concentration on the formation of cellulose II. Study by X-ray diffraction and FTIR spectroscopy," *Holzforschung* 49(6), 505-511. https://doi.org/10.1515/hfsg.1995.49.6.505

Gong, X., Li, Q., Li, T., Li, C., Huang, J., Zhou, N., and Jia, X. (2022). "Chemical composition and monolignin in alkali and acid treated corncob affect sugar release," *Industrial Crops and Products* 176, article ID 114317. https://doi.org/10.1016/j.indcrop.2021.114317

Guida, M. Y., Rebbah, B., Anter, N., Medaghri-Alaoui, A., Rakib, E. M., and Hannioui, A. (2021). "Biofuels and biochars production from agricultural biomass wastes by thermochemical conversion technologies: Thermogravimetric analysis and pyrolysis studies," *Progress in Agricultural Engineering Sciences* 17(1), 15-36. https://doi.org/10.1556/446.2021.00020

Haliman, A. C., Yuliati, S., and Hasan, A. (2025). "Synthesis and characterization of microcrystalline cellulose (MCC) from corn waste (*Zea mays* L.)," *Makara Journal of Science* 29(3), 10. https://doi.org/10.7454/mss.v29i3.2215

Hamid, A., Zafar, A., Latif, S., Peng, L., Wang, Y., Liaqat, I., Afzal, M. S., ul-Haq, I., and Aftab, M. N. (2023). "Enzymatic hydrolysis of low temperature alkali pretreated wheat straw using immobilized β-xylanase nanoparticles," *RSC Advances* 13(2), 1434-1445. https://doi.org/10.1039/D2RA07231A

Hussain, M. S., Shi, M., Zhang, S., Zhang, Y., Bie, X., Li, Q., Zhang, Y., Lubjuhn, S., Venghaus, S., and Zhou, H. (2025). "Techno-economic and life-cycle assessments of biomass thermochemical conversion into gaseous fuels," *Energy & Environment Nexus* 1(1), article e014. https://doi.org/10.48130/een-0025-0015

Kim, J. S., Lee, Y. Y., and Kim, T. H. (2016). "A review on alkaline pretreatment technology for bioconversion of lignocellulosic biomass," *Bioresource Technology* 199, 42-48. https://doi.org/10.1016/j.biortech.2015.08.085

Kim, S., Hwang, K., Lee, J., Chun, S. J., Lee, D., Kim, Y., Lee, D., and Gwon, J. (2025). "Contribution of structural changes in cellulose fibers induced by alkali treatment to their nanofibrillation," *ACS Omega* 10(41), 49087-49097. https://doi.org/10.1021/acsomega.5c07902

Li, Y., An, N., Cao, H., Shen, Z., Song, Y., and Tang, Y. (2025). "Strategic pretreatment tailoring biomass catalytic pyrolysis: Unraveling the synergy between physicochemical modification and reaction kinetics for sustainable biofuel production," *Journal of the Energy Institute*, article 102388. https://doi.org/10.1016/j.joei.2025.102388

Lin, H., Guo, X., Ding, K., Li, D., Zhang, H., Jia, X., Zhang, H., Zhou, L., Han, L., Liu, X., and Xiao, W. (2024). "Effect of alkali and ball milling on enhancing biomass depolymerization in the combined mechanochemical catalysis," *Industrial Crops and Products* 222, article 119819. https://doi.org/10.1016/j.indcrop.2024.119819

Liu, N., Huang, H., Feng, J., Li, R., Huang, X., and Wu, Y. (2025). "Effects of alkali and alkaline earth metals in biomass on co-pyrolysis characteristics and product distribution of coal and biomass," *Fuel* 389, article 134551. https://doi.org/10.1016/j.fuel.2025.134551

Liu, Y., Li, Z., Floess, E., Zhang, Y., Lam, N., Mawusi, S. K., Shrestha, P., Li, X., Xue, C., and Liu, G. (2023). "Field assessment of straw pellet combustion in improved

heating stoves in rural Northeast China," *Journal of Environmental Sciences* 127, 295-307. https://doi.org/10.1016/j.jes.2022.05.046

Lu, X., and Gu, X. (2022). "A review on lignin pyrolysis: Pyrolytic behavior, mechanism, and relevant upgrading for improving process efficiency," *Biotechnology for Biofuels and Bioproducts* 15(1), article 106. https://doi.org/10.1186/s13068-022-02203-0

Ma, H. L., Zhang, Y. C., Xu, F. X., Ma, N. F., Li, M. F., Wang, G. H., Huang, M. J., Fang, Z., and Jiang, L. Q. (2025a). "Fast pyrolysis and enzymatic hydrolysis of bagasse cellulose from synergistic alkaline and oxidative pretreatment," *Renewable Energy* 256(Part G), article 124426. https://doi.org/10.1016/j.renene.2025.124426

Ma, H. L., Xu, F. X., Zhang, Y. C., Huang, M. J., Li, M. F., Wang, G. H., Huang, M. X., Fang, Z., and Jiang, L. Q. (2025b). "Non-unified effects of cellulose allomorphs on fast pyrolysis and enzymatic hydrolysis," *Industrial Crops and Products* 230, article 121153. https://doi.org/10.1016/j.indcrop.2025.121153

Ma, Y., Li, H., Yang, H., Zhu, Y., Zhao, L., and Li, M. (2022). "Effects of solid acid and base catalysts on pyrolysis of rice straw and wheat straw biomass for hydrocarbon production," *Journal of the Energy Institute* 101, 140-148. https://doi.org/10.1016/j.joei.2021.08.010

Makhado, E., Seleka, W. M., Mahlaule-Glory, L., Selowa, K., Elella, M. H. A., Botlhoko, O. J., Satekge, T. K., and Hato, M. J. (2025). "Comparative extraction and characterisation of cellulose nanostructures from sawdust and maize stalk biomass," *International Journal of Biological Macromolecules* 329(Part 1), article 147842. https://doi.org/10.1016/j.ijbiomac.2025.147842

Memon, T. A., Vasudev, V., Ram, S., Keerio, H. A., and Kumar, S. (2026). "Synergistic effects during the co-pyrolysis of rice straw and pinewood sawdust: Investigation of thermal decomposition behavior and reaction kinetics," *Chemical Engineering Communications* 2026, 1-14. https://doi.org/10.1080/00986445.2025.2611399

Muigai, H. H., Choudhury, B. J., Kalita, P., and Moholkar, V. S. (2020). "Co-pyrolysis of biomass blends: Characterization, kinetic and thermodynamic analysis," *Biomass and Bioenergy* 143, article 105839. https://doi.org/10.1016/j.biombioe.2020.105839

Pasca Supanta, E., Félix, L. L., Pacheco-Salazar, D. G., and Gutiérrez-Pineda, E. (2025). "Ultrasound-assisted alkaline hydrogen peroxide pretreatment for biopolymer recovery from exhausted purple corn cobs," *ACS Omega* 10(44), 52634-52647. https://doi.org/10.1021/acsomega.5c06039

Pitchai, T., Babu, R., Ramanujam, S., and Kuttalam, I. (2019). "Thermogravimetric and kinetic study of pyrolysis of corn cob biomass," *Journal of Renewable Energy and Environment* 6(4), 35-40. https://doi.org/10.30501/JREE.2019.102816

Ramírez-Estrada, A., Mena-Cervantes, V. Y., Elizalde-Martínez, I., Pineda-Flores, G., and Hernández-Altamirano, R. (2024). "Chemical pretreatment of corncob for the selective dissolution of hemicellulose and lignin: influence of pretreatment on the chemical, morphological and thermal features," *Biofuels* 15(1), 89-103. https://doi.org/10.1080/17597269.2023.2219484

Rosu, L., Varganici, C. D., Crudu, A. M., and Rosu, D. (2018). "Influence of different tanning agents on bovine leather thermal degradation," *Journal of Thermal Analysis and Calorimetry* 134(1), 583-594. https://doi.org/10.1007/s10973-018-7076-3

Salami, H. A., Morales-Mendoza, J. E., Domínguez-Arvizu, J. L., Gaxiola-Cebreros, F. A., Hernández-Majalca, B. C., Bueno-Escobedo, J. L., Alalade, I. J., Valenzuela-Castro, G. E., Pérez-Hernández, L., López-Ortiz, A., *et al.* (2025). "Beyond the peak

temperature: An experimental evaluation of conventional *vs.* effective thermodynamic models for biomass pyrolysis," *Journal of the Energy Institute* 123, article 102333. https://doi.org/10.1016/j.joei.2025.102333

Salema, A. A., Ting, R. M. W., and Shang, Y. K. (2019). "Pyrolysis of blend (oil palm biomass and sawdust) biomass using TG-MS," *Bioresource Technology* 274, 439-446. https://doi.org/10.1016/j.biortech.2018.12.014

Sankhla, S., Mondal, S., and Neogi, S. (2023). "Pyrolysis of cellulose nanofibers: detailed assessment of process kinetics and thermodynamic parameters," *Cellulose* 30(12), 7695-7712. https://doi.org/10.1007/s10570-023-05379-2

Segal, L. G. J. M. A., Creely, J. J., Martin, Jr, A. E., and Conrad, C. M. (1959). "An empirical method for estimating the degree of crystallinity of native cellulose using the X-ray diffractometer," *Textile Research Journal* 29(10), 786-794. https://doi.org/10.1177/004051755902901003

Sethi, N., Luhach, N., Kirrolia, A. S., Gupta, A., Bishnoi, N. R., Dhull, S. B., and Rose, P. K. (2024). "Physicochemical characterization of rice straw before and after alkali-assist photocatalytic pretreatment: A comparative analysis," *Environmental Science and Pollution Research* 32, 29581-29591. https://doi.org/10.1007/s11356-024-33647-6

Silos-Llamas, A. K., Sudibyo, H., Hernández-Montoya, V., Meredith, W., and Durán-Jiménez, G. (2023). "Fast pyrolysis of agricultural residues: Reaction mechanisms and effects of feedstock properties and microwave operating conditions on the yield and product composition," *Journal of Analytical and Applied Pyrolysis* 175, article 106217. https://doi.org/10.1016/j.jaap.2023.106217

Singh, R. K., Patil, T., Verma, A., Tekade, S. P., and Sawarkar, A. N. (2021). "Insights into kinetics, reaction mechanism, and thermodynamic analysis of pyrolysis of rice straw from rice bowl of India," *Bioresource Technology Reports* 13, article 100639. https://doi.org/10.1016/j.biteb.2021.100639

Sluiter, A., Hames, B., Ruiz, R., Scarlata, C., Sluiter, J., Templeton, D., and Crocker, D. L. A. P. (2008). "Determination of structural carbohydrates and lignin in biomass," *Lab. Anal. Proced* 1617(1), 1-16.

Song, D. Y., and Lee, J. W. (2024). "Valorization of biochar and lignin derived from the NaOH pretreatment of lignocellulosic biomass for applications as an adsorbent and antioxidant," *Biomass & Bioenergy* 182, article 107103. https://doi.org/10.1016/j.biombioe.2024.107103

Stanciu, M. C., Tanasă, F., and Teacă, C. A. (2025). "Crystallinity changes in modified cellulose substrates evidenced by spectral and X-ray diffraction data," *Polysaccharides* 6(2), article 30. https://doi.org/10.3390/polysaccharides6020030

Stachowiak-Wencek, A., Zborowska, M., Waliszewska, H., and Waliszewska, B. (2019). "Chemical changes in lignocellulosic biomass (corncob) influenced by pretreatment and anaerobic digestion (AD)," *BioResources* 14(4), 8082-8099. https://doi.org/10.15376/biores.14.4.8082-8099

Suriapparao, D. V., and Vinu, R. (2018). "Effects of biomass particle size on slow pyrolysis kinetics and fast pyrolysis product distribution," *Waste and Biomass Valorization* 9(3), 465-477. https://doi.org/10.1007/s12649-016-9815-7

Ting, Z. J., Raheem, A., Dastyar, W., Yang, H., Dong, W., Yuan, H., Li, X., Wang, W., Zhang, R., and Zhao, M. (2020). "Alkaline pyrolysis of anaerobic digestion residue with selective hydrogen production," *International Journal of Hydrogen Energy* 45(41), 20933-20943. https://doi.org/10.1016/j.ijhydene.2020.05.278

Tsegaye, B., Balomajumder, C., and Roy, P. (2019). "Alkali pretreatment of wheat straw

followed by microbial hydrolysis for bioethanol production," *Environmental Technology* 40(9), 1203-1211. https://doi.org/10.1080/09593330.2017.1418911

Vilas-Boas, A. C. M., Tarelho, L. A. C., Oliveira, H. S. M., Silva, F. G. C. S., Pio, D. T., and Matos, M. A. A. (2024). "Valorisation of residual biomass by pyrolysis: Influence of process conditions on products," *Sustainable Energy & Fuels* 8(2), 379-396. https://doi.org/10.1039/D3SE01216F

Vyazovkin, S. (2024). "Misinterpretation of thermodynamic parameters evaluated from activation energy and preexponential factor determined in thermal analysis experiments," *Thermo* 4(3), 373-381. https://doi.org/10.3390/thermo4030019

Vyazovkin, S., Burnham, A. K., Criado, J. M., Pérez-Maqueda, L. A., Popescu, C., and Sbirrazzuoli, N. (2011). "ICTAC Kinetics Committee recommendations for performing kinetic computations on thermal analysis data," *Thermochimica Acta* 520(1-2), 1-19. https://doi.org/10.1016/j.tca.2011.03.034

Vyazovkin, S., Chrissafis, K., Di Lorenzo, M. L., Koga, N., Pijolat, M., Roduit, B., Sbirrazzuoli, N., and Suñol, J. J. (2014). "ICTAC Kinetics Committee recommendations for collecting experimental thermal analysis data for kinetic computations," *Thermochimica Acta* 590, 1-23. https://doi.org/10.1016/j.tca.2014.05.036

Waluyo, J., Purba, I. T., Linanggeng, Z. A., Maulana, M. L., Kanchanatip, E., Yan, M., and Hantoko, D. (2025). "Biomass pyrolysis: A comprehensive review of production methods, derived products, and sustainable applications in advanced materials," *Applied Science and Engineering Progress* 18(2), 7645-7645. https://doi.org/10.14416/j.asep.2024.11.009

Wang, L., Fan, J., Gan, L., Zeng, X., Lin, L., and Liu, J. (2024). "Thermostatic microwave-assisted pretreatment of corn stover at atmospheric pressure to enhance saccharification," *Biomass and Bioenergy* 188, article 107343. https://doi.org/10.1016/j.biombioe.2024.107343

Wang, J., Ding, L., Sun, Z., Guo, Q., Gong, Y., and Yu, G. (2025b). "Release behaviors and catalytic effects of alkali and alkaline earth metals in coke from rapid pyrolysis of wheat straw," *Journal of Analytical and Applied Pyrolysis* 190, article 107160. https://doi.org/10.1016/j.jaap.2025.107160

Wang, S., Hu, Y., and Wang, Y. (2025a). "Pyrolysis of rice straw for bioenergy: Kinetics, reaction mechanism, and by-products using TG and Py-GC/MS analysis," *Journal of Thermal Science and Technology* 20(1), article 24-00395. https://doi.org/10.1299/jtst.24-00395

Wang, Z., Zhang, C., Xia, S., and Dong, Y. (2025c). "*In-situ* catalytic pyrolysis of biomass using low-dose alkali metal salts: The effect of salt type and temperature," *Journal of the Energy Institute* 119, article 102012. https://doi.org/10.1016/j.joei.2025.102012

Wang, W., Lemaire, R., Bensakhria, A., and Luart, D. (2022). "Review on the catalytic effects of alkali and alkaline earth metals (AAEMs) including sodium, potassium, calcium and magnesium on the pyrolysis of lignocellulosic biomass and on the co-pyrolysis of coal with biomass," *Journal of Analytical and Applied Pyrolysis* 163, article 105479. https://doi.org/10.1016/j.jaap.2022.105479

Wei, F., Cao, J. P., Zhao, J. P., and Zhao, X. Y. (2025). "Unlocking biofuel potential: Synergistic production of biofuel precursors from acid-loaded corncobs *via* staged pyrolysis," *Journal of Analytical and Applied Pyrolysis* 188, article 107059. https://doi.org/10.1016/j.jaap.2025.107059

Woźniak, M., Ratajczak, I., Wojcieszak, D., Waśkiewicz, A., Szentner, K., Przybył, J., Borysiak, S., and Goliński, P. (2021). "Chemical and structural characterization of maize stover fractions in aspect of its possible applications," *Materials* 14(6), article 1527. https://doi.org/10.3390/ma14061527

Xia, S., Zheng, A., Zhao, K., Zhao, Z., and Li, H. (2022). "Evaluation of pyrolysis reactivity, kinetics, and gasification reactivity of corn cobs after torrefaction pretreatment," *Energies* 15(24), article 9277. https://doi.org/10.3390/en15249277

Yang, H., Chen, Z., Zhang, Y., Liu, B., Yang, Y., Tang, Z., Chen, Y., and Chen, H. (2024). "Catalytic effect of K and Na with different anions on lignocellulosic biomass pyrolysis," *Frontiers of Chemical Science and Engineering* 18(12), article 141. https://doi.org/10.1007/s11705-024-2492-3

Yahya, A. M., Adeleke, A. A., Nzerem, P., Ikubanni, P. P., Ayuba, S., Rasheed, H. A., Gimba, A., Okafor, I., Okolie, J. A., and Paramasivam, P. (2023). "Comprehensive characterization of some selected biomass for bioenergy production," *ACS Omega* 8(46), 43771-43791. https://doi.org/10.1021/acsomega.3c05656

Yılbaşı, Z. (2025). "Biofuels, e-fuels, and waste-derived fuels: Advances, challenges, and future directions," *Sustainability* 17(13), article 6145. https://doi.org/10.3390/su17136145

Yu, L., Shi, X., Zhang, S., Zhang, Q., and Chen, W. (2025). "A comprehensive investigation of kinetic and thermodynamic analysis to catalytic pyrolysis bamboo with N-doped biochar," *Fuel* 396, article 135312. https://doi.org/10.1016/j.fuel.2025.135312

Yuan, S., Tan, Z., and Huang, Q. (2018). "Migration and transformation mechanism of nitrogen in the biomass-biochar-plant transport process," *Renewable and Sustainable Energy Reviews* 85, 1-13. https://doi.org/10.1016/j.rser.2018.01.008

Yunpu, W., Zhang, S., Yu, Z., Jiang, L., Liu, Y., Ruan, R., and Fu, G. (2018). "Conversion of biomass to hydrocarbon-rich bio-oil *via* microwave-assisted catalytic pyrolysis: A review," *China Petroleum Processing and Petrochemical Technology* 20(3), 7-16.

Zhang, H., Liu, M., Yang, Y., Chen, W., Zhu, J., Zhang, S., Yang, H., Chen, H., and Chen, Y. (2023). "Mechanism study on the interaction between holocellulose and lignin during secondary pyrolysis of biomass: In terms of molecular model compounds," *Fuel Processing Technology* 244, article 107701. https://doi.org/10.1016/j.fuproc.2023.107701

Zhang, H., Jia, X., Ding, K., Liang, X., He, Y., Guo, X., Zhou, L., Han, L., and Xiao, W. (2025a). "Optimizing lignocellulose conversion: A comparative study of alkali-assisted ball milling pretreatment of cotton stalk and corn stover," *Journal of Biotechnology* 408,15-27. https://doi.org/10.1016/j.jbiotec.2025.08.018.

Zhang, X., Zhang, Y., Zhang, S., Yao, L., and Hao, Y. (2025b). "Lignocellulosic biomass pyrolysis: A review on the pretreatment and catalysts," *Fuel Processing Technology* 279, article 108352. https://doi.org/10.1016/j.fuproc.2025.108352

Zheng, A., Zhao, K., Li, L., Zhao, Z., Jiang, L., Huang, Z., Wei, G., He, F., and Li, H. (2018). "Quantitative comparison of different chemical pretreatment methods on chemical structure and pyrolysis characteristics of corncobs," *Journal of the Energy Institute* 91(5), 676-682. https://doi.org/10.1016/j.joei.2017.06.002

Article submitted: March 29, 2026; Peer review completed: May 4, 2026; Revised version received and accepted: June 5, 2025: Published: June 16, 2026.
DOI: 10.15376/biores.21.3.6975-7005

APPENDIX

Supplementary Materials

S1. Co-pyrolysis Kinetic Theory

Generally, the reaction rate of solid materials during non-isothermal degradation can be described by the following Eqs. S1 and S2 (Galwey and Brown 1998),

$$\frac{d\alpha}{dt} = A\exp\left(-\frac{E_\alpha}{RT}\right)f(\alpha) \quad (S1)$$

$$\alpha = \frac{m_0 - m_t}{m_0 - m_f} \quad (S2)$$

where α is the conversion rate, which can be calculated by the Eq. S2; m_0, m_f, and m_t are the initial mass of sample, the final mass of sample, and the actual mass of sample at pyrolysis time of t, respectively. A is the pre-exponential factor (s^{-1}); E_α is the activation energy (kJ/mol); R is the gas constant (8.31 J/ mol•K), T is the Kelvin temperature (K), f(α) is a function of reaction model reflecting the pyrolysis mechanism.

At a constant heating rate (β=dT/dt) under non-isothermal conditions, Eq. S1 can be rewritten as Eq. S3.

$$\beta\frac{d\alpha}{dT} = A\exp\left(-\frac{E_\alpha}{RT}\right)f(\alpha) \quad (S3)$$

The integral form of Eq. S3 is given by Eq. S4.

$$g(\alpha) = \int_0^\alpha \frac{d\alpha}{f(\alpha)} = \frac{A}{\beta}\int_0^T \exp\left(-\frac{E_\alpha}{RT}\right)dT = \frac{AE_\alpha}{\beta R}P\left(\frac{E}{RT}\right) \quad (S4)$$

In this study, model-free methods (KAS and FR) and model-fitting method (Criado) were employed to calculate the pyrolysis activation energy and mechanism (Friedman 1964; Ozawa 1965; Flynn and Wall 1966; Hu *et al.* 2020).

The KAS method based on the Coats-Redfern approximation (Coats and Redfern 1964) is an integral isoconversional method, which is defined as Eq. S5. Therefore, E_α can be obtained from the slope of the straight line by plotting *lnβ versus 1/T*.

$$\ln\beta/T^2 = -\frac{E_\alpha}{RT} - \ln\left[\frac{E_\alpha}{AR}g(\alpha)\right] \quad (S5)$$

The equation of FR method is obtained by taking the natural logarithm of both sides of Eq. S3, which is defined as Eq. S6. It is easy to obtain the E_α value by plotting ln (β•dα/dT) against 1/T.

$$\ln\left(\beta\frac{d\alpha}{dT}\right) = \ln\left[Af(\alpha)\right] - \frac{E_\alpha}{RT} \quad (S6)$$

Criado method is typically employed to determine the pyrolysis mechanism of solid materials, which is expressed in Eq. S7 (Criado *et al*. 1989).

$$Z(\alpha)=\frac{d\alpha/dT}{\beta}\pi(\chi)T \quad \text{(S7)}$$

In Eq. S7, $\chi = E_\alpha/RT$ and $\pi(\chi)$ is an approximation of the temperature integral, which is difficult to be expressed in a simple mathematical formula. Hence, it is usually expressed by Senum and Yang's fourth rational expression ($p(\chi)$) (Pérez-Maqueda and Criado 2000). Equation S8 obtained from the rearrangement of Eq. S7 is used to plot the experimental cure. Master curves of different models in Table S1 was plotted from Eq. S9, which is commonly used to describe the theoretical solid-state reactions with no need to consider the kinetic parameters. The pyrolysis mechanism of the samples can be determined by comparing the experimental curves with the master curves of different models.

$$Z(\alpha)=\frac{d\alpha}{dT}\left(\frac{E_\alpha}{R}\right)\exp\left(\frac{E_\alpha}{RT}\right)P(\chi) \quad \text{(S8)}$$

$$Z(\alpha)=f(\alpha)g(\alpha) \quad \text{(S9)}$$

Table S1. Function Expressions of the Most Common Reaction Mechanisms in Solid Reactions*

Kinetic Mechanism	$f(\alpha)$	$g(\alpha)$	Reaction Order
A2, Nucleation and growth (Avrami Eq. 1)	$2(1-\alpha)[-\ln(1-\alpha)]^{1/2}$	$[-\ln(1-\alpha)]^{1/2}$	n=1/2
A3, Nucleation and growth (Avrami Eq. 2)	$3(1-\alpha)[-\ln(1-\alpha)]^{2/3}$	$[-\ln(1-\alpha)]^{1/3}$	n=1/3
A4, Nucleation and growth (Avrami Eq. 3)	$4(1-\alpha)[-\ln(1-\alpha)]^{3/4}$	$[-\ln(1-\alpha)]^{1/4}$	n=1/4
R1, Phase boundary controlled reaction (one-dimensional movement)	1	α	n=1
R2, Phase boundary controlled reaction (contracting area)	$2(1-\alpha)^{1/2}$	$[1-(1-\alpha)^{1/2}]$	n=2
R3, Phase boundary controlled reaction (contracting volume)	$3(1-\alpha)^{2/3}$	$[1-(1-\alpha)^{1/3}]$	n=3
D1, One-dimensional diffusion	$1/2\alpha$	α^2	Parabolic law
D2, Two-dimensional diffusion (Valensi)	$[-\ln(1-\alpha)]^{-1}$	$[(1-\alpha)\ln(1-\alpha)]+\alpha$	Valensi equation
D3, Three-dimensional diffusion (Jander)	$3(1-\alpha)^{2/3}/[2(1-(1-\alpha)^{1/3})]$	$[1-(1-\alpha)^{1/3}]^2$	Jander equation n=2
F1, Random nucleation with one nucleus on the individual particle	$1-\alpha$	$-\ln(1-\alpha)$	n=1
F2, Random nucleation with two nuclei on the individual particle	$(1-\alpha)^2$	$(1-\alpha)^{-1}$	n=2
F3, Random nucleation with three nuclei on the individual particle	$1/2(1-\alpha)^3$	$(1-\alpha)^{-2}$	n=3

*Saha *et al*. 2008; Ma *et al*. 2018; Gotor *et al*. 2000

S2. Estimation of Thermodynamic Parameters

The pre-exponential factor (A) in the Arrhenius equation was calculated according to Eq. S10 using the activation energies obtained from the KAS and FR methods, where T_m represents the peak temperature of the DTG curve. Thermodynamic parameters of Gibbs free energy change (ΔG), enthalpy change (ΔH), and entropy change (ΔS) are derived from Eqs. S11 to S13 (ASTM E698–79 1993; Pourmortazavi *et al.* 2007).

$$A = \beta E_\alpha \exp\left(\frac{E_\alpha}{RT_m}\right) / RT_m^2 \quad \text{(S10)}$$

$$\Delta G = E_\alpha + RT_m \ln\left(\frac{K_B T_m}{hA}\right) \quad \text{(S11)}$$

$$\Delta H = E_\alpha - RT_m \quad \text{(S12)}$$

$$\Delta S = \frac{\Delta H - \Delta G}{T_m} \quad \text{(S13)}$$

In Eq. S11, K_B is the Boltzmann constant(1.38×10^{-23} J/K), and h is the Plank constant (6.63×10^{-34} J·s).

S3. Chemical Structures of Pyrolysis Products

The composition and chemical structure of the pyrolysis products of SA and SB are shown in Table S2.

Table S2. Pyrolysis Compositions and Chemical Structure of Samples Obtained from Py-GC/MS at 550 °C

Sample	No.	Component	Chemical Structures
SA	1	Carbon dioxide	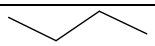
	2	n-Butane	
	3	2,3-Butanedione	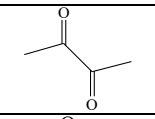
	4	Acetic acid	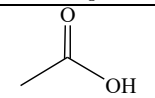
	5	Hydroxyacetone	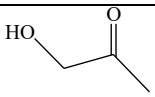
	6	Methyl pyruvate	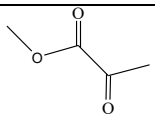
	7	Succindialdehyde	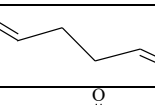
SA	8	Ethyl pyruvate	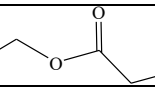

	9	4,5-Dimethylimidazole	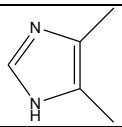
	10	3-Methyl-2-heptanone	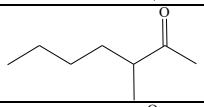
	11	1-(acetyloxy)-2-Propanone	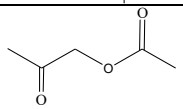
	12	2(5H)-Furanone	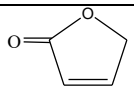
	13	Cyclohexanone	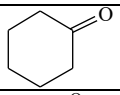
	14	7-Oxabicyclo[2.2.1]heptan-2-one	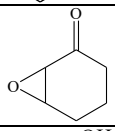
	15	cis-1,2-Dihydrocatechol	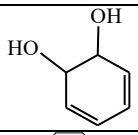
	16	Cyclooctane	
	17	2-methoxy-Phenol	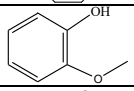
	18	Cyclopropyl carbinol	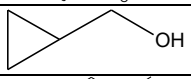
	19	3,6-Dimethyl-tetrahydropyran-2-one	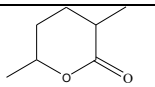
	20	dihydro-2H-Pyran-3(4H)-one	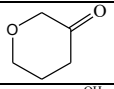
	21	2-ethyl-Phenol	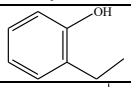
	22	1-Methylhexyl hydroperoxide	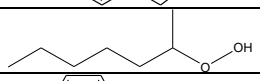
	23	Phenoxyethene	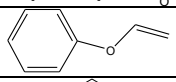
	24	4-ethyl-2-methoxy-Phenol	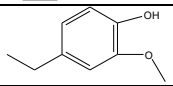
	25	4-vinyl-2-methoxy-Phenol	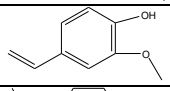
	26	2,4-Dimethoxyphenol	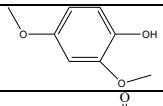
	27	4-Hydroxy-2-methoxybenaldehyde	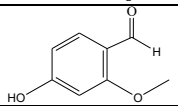
SA	28	2-methoxy-4-propenyl-Phenol	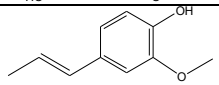

	29	4-(3-hydroxy-1-propenyl)-2-methoxy-Phenol	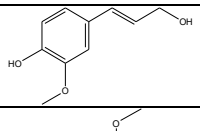
	30	4-allyl-2,6-dimethoxy-Phenol	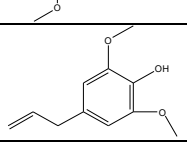
SB	1	Carbon dioxide	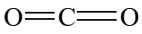
	2	n-Butane	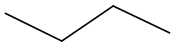
	3	2,3-Butanedione	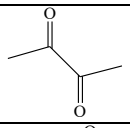
	4	2-Oxopropanoic acid	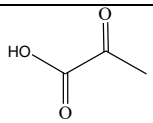
	5	Hydroxyacetone	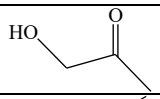
	6	3,4-Dimethyl-1H-pyrazole	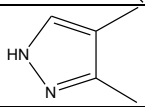
	7	2-Methyl-2-cyclopentenone	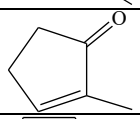
	8	Butyrolactone	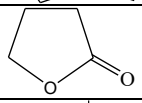
	9	2-Methyl-2-cyclopentenone	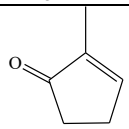
	10	3-Methylcyclopentane-1,2-dione	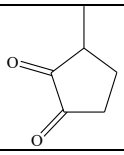
	11	(Z)-2-Undecene	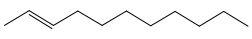
	12	2-methoxy-Phenol	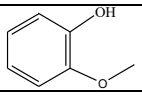
	13	Cyclopropyl carbinol	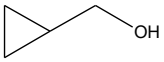
	14	4-Ethylcyclohexanone	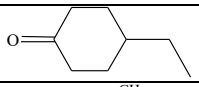
	15	2-Methylenecyclohexanol	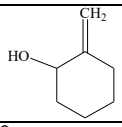
	16	(ethenyloxy)-Benzene	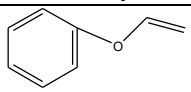

	17	4-ethyl-2-methoxy-Phenol	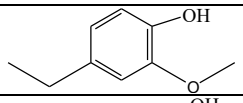
	18	2-Methoxy-4-vinylphenol	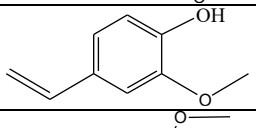
	19	2,4-Dimethoxyphenol	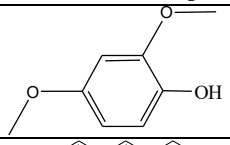
	20	4-(3-hydroxy-1-propenyl)-2-methoxy-Phenol	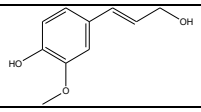

REFERENCES CITED

ASTM E698–79 (1993). "Standard test method for Arrhenius kinetic constants for thermally unstable materials," ASTM International, West Conshohocken, PA, USA.

Coats, A. W., and Redfern, J. P. (1964). "Kinetic parameters from thermogravimetric data," *Nature* 201(4914), 68-69. https://doi.org/10.1038/201068a0

Criado, J. M., Malek, J., and Ortega, A. (1989). "Applicability of the master plots in kinetic analysis of non-isothermal data," *Thermochimica Acta* 147(2), 377-385. https://doi.org/10.1016/0040-6031(89)85192-5

Flynn, J. H., and Wall, L. A. (1966). "General treatment of the thermogravimetry of polymers," *Journal of Research of the National Bureau of Standards. Section A, Physics and Chemistry* 70(6), article 487. https://doi.org/10.6028/jres.070A.043

Friedman, H. L. (1964). "Kinetics of thermal degradation of char-forming plastics from thermogravimetry. Application to a phenolic plastic," *Journal of Polymer Science Part C: Polymer Symposia* 6(1), 183-195. https://doi.org/10.1002/polc.5070060121

Galwey, A. K., and Brown, M. E. (1998). "Kinetic background to thermal analysis and calorimetry," *Principles and Practice* 1, 147-224.

Gotor, F. J., Criado, J. M., Malek, J., and Koga, N. (2000). "Kinetic analysis of solid-state reactions: The universality of master plots for analyzing isothermal and nonisothermal experiments," *The Journal of Physical Chemistry A* 104(46), 10777-10782. https://doi.org/10.1021/jp0022205

Hu, Y., Liu, J., Luo, L., Li, X., Wang, F., and Tang, K. (2020). "Kinetics and mechanism of thermal degradation of aldehyde tanned leather," *Thermochimica Acta* 691, article 178717. https://doi.org/10.1016/j.tca.2020.178717

Ma, Z., Wang, J., Yang, Y., Zhang, Y., Zhao, C., Yu, Y., and Wang, S. (2018). "Comparison of the thermal degradation behaviors and kinetics of palm oil waste under nitrogen and air atmosphere in TGA-FTIR with a complementary use of model-free and model-fitting approaches," *Journal of Analytical and Applied Pyrolysis* 134, 12-24. https://doi.org/10.1016/j.jaap.2018.04.002

Ozawa, T. (1965). "A new method of analyzing thermogravimetric data," *Bulletin of the Chemical Society of Japan* 38(11), 1881-1886. https://doi.org/10.1246/bcsj.38.1881

Pérez-Maqueda, L. A., and Criado, J. M. (2000). "The accuracy of Senum and Yang's approximations to the Arrhenius integral," *Journal of Thermal Analysis and Calorimetry* 60(3), 909-915. https://doi.org/10.1023/A:1010115926340

Pourmortazavi, S. M., Kohsari, I., Teimouri, M. B., and Hajimirsadeghi, S. S. (2007). "Thermal behaviour kinetic study of dihydroglyoxime and dichloroglyoxime," *Materials Letters* 61(25), 4670-4673. https://doi.org/10.1016/j.matlet.2007.03.041

Saha, B., Reddy, P. K., and Ghoshal, A. K. (2008). "Hybrid genetic algorithm to find the best model and the globally optimized overall kinetics parameters for thermal decomposition of plastics," *Chemical Engineering Journal* 138(1-3), 20-29. https://doi.org/10.1016/j.cej.2007.05.024